Theoretical hardness analysis and experimental verification for SiAlON based nano-composites

Author

MUHAMMAD ZUBAIR

00000273564

Supervisor

Dr. BILAL AHMED ANJUM

DEPARTMENT OF MECHANICAL ENGINEERING

COLLEGE OF ELECTRICAL & MECHANICAL ENGINEERING

NATIONAL UNIVERSITY OF SCIENCES AND TECHNOLOGY

ISLAMABAD

FEB, 2021

Theoretical hardness analysis and experimental verification for SiAlON based nano-composites

Author

MUHAMMAD ZUBAIR

00000273564

A thesis submitted in partial fulfillment of the requirements for the degree of

MS Mechanical Engineering

Thesis Supervisor:

Dr. BILAL AHMED ANJUM

DEPARTMENT OF MECHANICAL ENGINEERING

COLLEGE OF ELECTRICAL & MECHANICAL ENGINEERING

NATIONAL UNIVERSITY OF SCIENCES AND TECHNOLOGY,

ISLAMABAD

FEB, 2021

Declaration

I certify that this research work titled "*Theoretical hardness analysis and experimental verification for SiAlON based nano-composites"* is my own work. The work has not been presented elsewhere for assessment. The material that has been used from other sources it has been properly acknowledged / referred.

Muhammad Zubair

00000273564
MS-2018 Mechanical Engineering
College of Electrical & Mechanical Engineering
National University of Sciences and Technology, Islamabad

Language Correctness Certificate

This thesis has been read by an English expert and is free of typing, syntax, semantic, grammatical and spelling mistakes. Thesis is also according to the format given by the university.

Muhammad Zubair

00000273564
MS-2018 Mechanical Engineering
College of Electrical & Mechanical Engineering
National University of Sciences and Technology, Islamabad

Dr. Bilal Ahmed Anjum

Assistant Professor
Department of Mechanical Engineering
College of Electrical & Mechanical Engineering
National University of Sciences and Technology, Islamabad

Copyright Statement

Copyright © 2021 by Muhammad Zubair

All rights reserved. Reproduction, distribution, or transmission of this thesis, in whole or in part in any form or by any means requires the prior written permission of the author. Copies (by any process) either in full, or of extracts, may be made only in accordance with instructions given by the author and lodged in the Library of NUST College of E&ME, details of which may be obtained from the Librarian. This page must form part of any such copies made. Further copies (by any process) may not be made without the permission (in writing) of the author.

The ownership of any intellectual property rights which may be described in this thesis is vested in NUST College of E&ME, subject to any prior agreement to the contrary, and may not be made available for use by third parties without the written permission of the College of E&ME, which will prescribe the terms and conditions of any such agreement.

Further information on the conditions under which disclosure and exploitation may take place is available from the Library of NUST College of E&ME, Rawalpindi

Acknowledgements

All praises, and thanks to **ALMIGHTY ALLAH**, the most Gracious, the most Merciful who granted me the strength to perform to the utmost of my abilities and with Whose will all of this was possible. Millions of Darood-o-Salam for **HAZRAT MUHAMMAD** (S.A.W.W.), who is an ever guiding a role model of guidance and knowledge for all the humanity.

I present my deepest gratitude to my Thesis Supervisor **Dr. Bilal Ahmed Anjum** for accommodating me, with his expertise and knowledge, at every step and turn of the whole ordeal. Despite his busy routine and having his hands full, he took me up, and actively guided and motivated me regarding everything in the thesis with his creative ideas.

I would acknowledge my sincere appreciation to **Dr. Raja Amer Azim**, the **Head of Department** of the Mechanical Department, whose deep insight and understanding of my situation made my thesis possible. He has always provided me with an inspiring attitude and exceptional guidance.

I am greatly indebted to my **friends and family**, especially **mother** who helped me at every step of this process, for their love support and countless prayers.

Devoted to my loving parents and younger brother whose never ending support and motivation made me accomplish this demanding yet beautiful journey

Abstract

SiAlON is a commercially important family of ceramics. These are based upon silicon nitride and inherit much of the useful properties like high fracture toughness and high hot hardness making it useful for harsh environments like automobile and gas turbine engines. Extensive research has been done on SiAlON to determine the effects of type of additives, composition of precursors, size of precursor particles, sintering techniques, heating and cooling rates etc. on SiAlON microstructure, phases and properties. SiAlON is continuously being made better by innovating and optimizing the above mentioned techniques and properties. A further step in the evolution of advance ceramics are SiAlON composites, in which different materials are used as a reinforcement in a SiAlON matrix to further enhance its properties. This area of research presents its own challenges like achieving complete densification even for high second phase content, preventing undesired phase transformations of second phase particles, achieving elongated grains of SiAlON in a composite etc. This review paper will attempt to comprehensively cover the latest techniques being utilized to improve the properties of SiAlON and then discuss the formation of promising SiAlON composites, their limitations and promising future work to make better SiAlON composites. This review paper will also calculate theoretical hardness of nanocomposites under study, relate their theoretically calculated and experimentally obtained values, and attempt at explaining the causes for the differences in these values.

Keywords: *SiAlON, SiAlON-ZrN Composites, SiAlON-SiC Composites, SiAlON-WC Composites, SiAlON-TiN Composites, Theoretical Hardness*

Table of Contents

List of Figures

List of Tables

Chapter # 1: Introduction

1.1: Overview

In 1970s, a new type of ceramics was formed whose structure was based upon Silicon Nitride (Si_3N_4) [1]. These were named as SiAlONs. Some of its properties include:

- High Hardness
- High Fracture toughness
- Wear resistance
- Hot hardness
- Creep resistance
- Thermal shock resistance
- Low density
- Low co-efficient of thermal expansion
- Low co-efficient of resistance [2,3]

Due to these properties, SiAlONs can be used in harsh conditions like automotive or gas turbine engines. Due to its numerous advantages over Silicon Nitride, SiAlONs are more widely used. Some of the uses of SiAlONs include:

- Cutting tools
- Engine valves
- Bearings
- Turbine vanes etc. [3,4]

1.2: Development

Si_3N_4 shows excellent performance to extreme thermal and medical conditions. A certain disadvantage of Si_3N_4 ceramics is that it requires very high temperature and lot of time for its complete densification. In order to ease the process, liquid phase sintering is carried out using metal oxides like MgO and Y_2O_3 [1]. This process has a certain disadvantage that when the liquid phase is cooled, a glassy phase is formed at grain boundaries which due to low resistance to creep and oxidation and vulnerable to chemical and mechanical degradation at high temperatures [6,7].
By forming a solid solution of Silver Nitride (AgN) and Aluminum Oxide(Al_2O_3) or Aluminum Nitride (AlN) and Silicon Oxide (SiO_2), SiAlON ceramics are formed [2]. SiAlON ceramics are also formed by densifying Si_3N_4 using different sintering additives like AlN, SiO_2 and Al_2O_3, as some of the Si- atoms are substituted by Al-atoms while N-atoms with O-atoms which are then incorporated in the crystal structure [7].

1.3: Phases

There are two main phases of SiAlON ceramics:

- α-SiAlON
- β-SiAlON

α-SiAlON is formed by forming solid solution of α-Si_3N_4 while β-SiAlON is formed by forming solid solution of β-Si_3N_4.
β-SiAlON was the first to be discovered among the two phases in 1970s. It is formed by substituting some Si-N bonds with Al-O bonds. General form of β-SiAlON is:

$$\mathbf{Si_{6-z}\text{-}Al_z\text{-}O_z\text{-}N_{8-z}} \qquad \textbf{(where z varies from 0 to 4.2)}$$

α-SiAlON is formed soon afterwards. In α-SiAlON, some of the Si-N bonds are substituted with Al-N and Al-O bonds. General form of α-SiAlON is:

$$\mathbf{M_x\ Si_{12-(m+n)}\ Al_{m+n}\ O_n\ N_{16-n}}$$

In this form:

- m represents Al-N bonds
- n represents Al-O bonds
- M represents a metal ion

Metal ion can be either Lithium (Li), Calcium (Ca), Magnesium (Mg) or any other rare earth metal apart from Europium (Eu), Lanthanum (La), Praseodymium(Pr), and Cerium (Ce). Metal ion's valency should be v+, while **m = v*x**. 'x' is also limited to equal or less than 2 (x<=2) due to only 2 interspatial spaces in each cell [1].
The metal ion is added in α-SiAlON as a stabilizer, since it equals the number of valence electrons caused due to the substitution to Si-N and Al-N atoms. For the substitution of Si-N and Al-O atoms, no such additives are required [3].

1.4: Structure of α-SiAlON and β-SiAlON

α-SiAlON has a similar trigonal structure like α-Si_3N_4, while β-SiAlON has a similar structure like β-Si_3N_4 which is hexagonal. In Si_3N_4, both phases are build up by corner sharing SiN_4 tetrahedra [8].

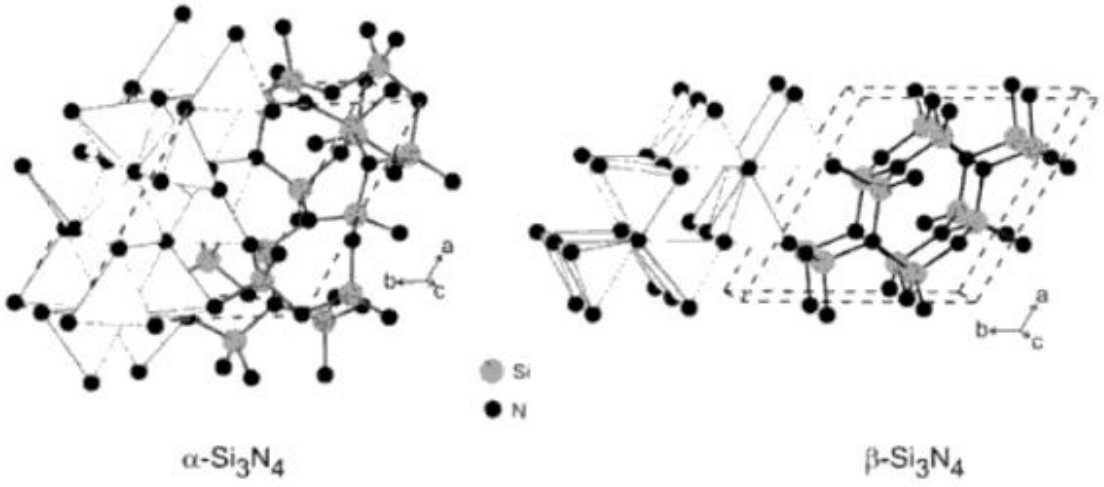

Figure 1.1: Crystal structure of α-Si3N4 and β-Si3N4.

In α-Si_3N_4, the Si and N atoms are arranged in ABABAB layer format while in β-Si_3N_4, the arrangement is in ABCABCABC layer format. In α-Si_3N_4 structure, cavities are formed while tunnels are formed in β-Si_3N_4 structure. By the substitution of some Al and O atoms, the overall structure of Si_3N_4 is not changed. Two Si_3N_4 units are present in a β-SiAlON unit cell while four Si_3N_4 units are present in an α-SiAlON unit cell with two interstitial spaces [3].

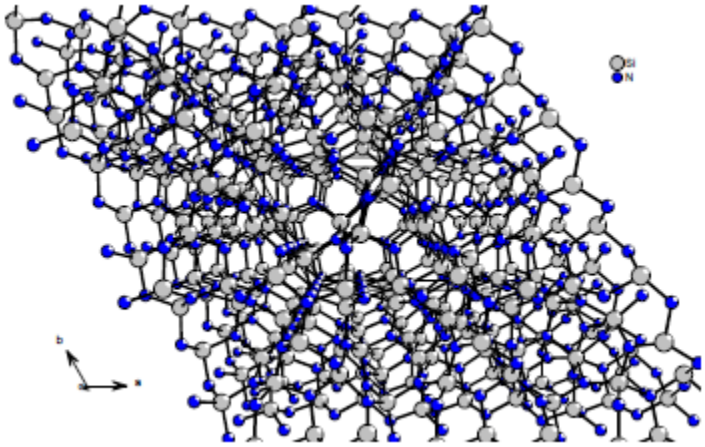

Figure 1.2: *Structure of α-SiAlON*

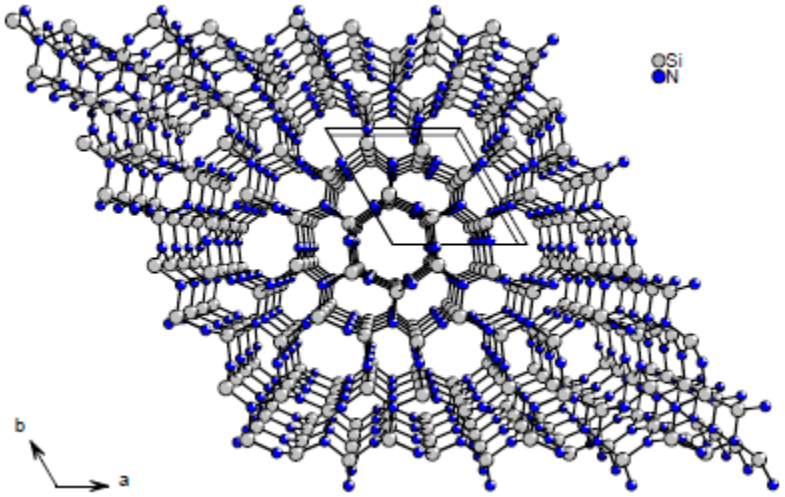

Figure 1.3: *Structure of β-SiAlON*

1.5: Microstructure

A lot of data is available for both α-SiAlON and β-SiAlON, but among these two, β-SiAlON is more widely used and accepted worldwide. One of the major reasons for the acceptance of β-SiAlON over α-SiAlON is its microstructure. β-SiAlON structure consists of whisker-like grain structure having aspect ratio of about 10 resulting in crack deflection and interlocking mechanisms which provides a greater fracture toughness β-SiAlON as compared to α-SiAlON. The structure for α-SiAlON is equiaxed grain structure. A method was introduced by forming α-β-SiAlON which utilizes the advantageous properties of both α-SiAlON (high hardness) and β-SiAlON (high fracture toughness) [9].
Anisotropic growth of α-SiAlON was observed around 1990s, which was dependent on the metal stabilizer's type used for the formation of α-SiAlON along with sintering conditions and precursor combinations. Presently, both α-SiAlON and β-SiAlON are used in cutting tools [10].

1.6: α- to β- Transformation

Some of the Si-N bonds are substituted by Al-N and Al-O bonds in α-SiAlON, resulting in the overall increase in the unit size of the cell. The bond length of Si-N bond is around 1.72 Å [3]. When Al-O bond is substituted, it has around the same bond length as Si-N bond so no major change is occurred in β-SiAlON but the bond length of Al-N bond is around 1.87 Å which is much higher than Si-N bonds resulting in distortion in the tetrahedral structure of α-SiAlON by

producing strain in the structure [7]. This strain helps α-SiAlON structure to transform from α- to β-SiAlON. α- to β-SiAlON transformation requires liquid phase and begins around 1400 ºC [1].

Chapter # 2: Theoretical Hardness of composite ceramics

Hardness of ceramic composites is greatly enhanced by the incorporation of nano reinforcements in contrast to micro-particles [11-12]. A lot of study has been done to theoretically calculate the hardness of composite ceramics in the past [13-20]. The hardness of the material mostly depends on the nature of chemical bonding within the region on which force is applied. Many different proposals have been reported to evaluate the theoretical hardness of ceramic composites [21-25]. The hardness of multi-component ceramics systems containing more than one kind of chemical bonding may well be calculated by considering the average contribution by all the constituents phases [26-32].

2.1: Analysis

Ceramic materials are mostly multi-component crystals. Their hardness is evaluated as as the average hardness of constituent phases. The hardness (H_v) of the multi-component can be shown as [29]:

$$H_v = \left[\prod_{1}^{\mu} (H_v^{\mu})^{n_\mu}\right]^{1/\sum n_\mu} \longrightarrow \quad \textbf{\textit{1}}$$

Where:

- μ is the nature of chemical bonding.
- n_μ is the total amount of μ-bonds having actual multi-component crystals.
- H_v^{μ} is the hardness of the individual material.

There are certain assumptions considered in evaluating using this model.

- There is no chemical interaction involved in the sintering process. This means no new phase is formed.
- The theoretical value obtained does not include the value of porosity.

Consider a composite consisting of a matrix phase (P_o) and the reinforcing phase (P_i), having mass fraction of c_o and c_i respectively. In parent material, there are p types of bonds and the number of bonds in a unit mole is n_j. Similarly, for the reinforcing phase, there are q_i types of bonds and the number of bonds in a unit mole is n_{ik}.

Hardness for matrix phase (H_v^{Po}) and adding phases (H_v^{Pi}) are as follows:

$$H_v^{P_0} = \left[\prod_{j=1}^{p} (H_v^j)^{n_j}\right]^{1/\sum n_j} \quad H_v^{P_i} = \left[\prod_{k=1}^{q_i} (H_v^k)^{n_{ik}}\right]^{1/\sum n_{ik}} \longrightarrow \mathbf{2}$$

The theoretical hardness for the composite ceramics material (H_v^{com}) can be written as:

$$H_v^{com} = \left[\prod_{1}^{m} (H_v^l)^{n_l}\right]^{1/\sum n_l} \longrightarrow \mathbf{3}$$

Where

- m is the total number of bonds
- n_l is the amount of one type of bonds present

Ratio of the amount of matrix chemical bonds to the reinforcing phase is,

$$N_0 = n_0 c_0 / M_0 N_i = n_i c_i / M_i \longrightarrow \mathbf{4}$$

- n_o is the number of bonds/mol of matrix phase
- n_i is the number of bonds/mol of adding phase
- c_o is the mass ratio of matrix phase
- c_i is the mass ratio of the reinforcing phase
- M_o is the relative molecular weight of matrix phase
- M_i is the relative molecular mass of reinforcing phase

The relative percentage of the bond in individual phases is:

$$c_{bi} = N_i / \sum_{0}^{n} N_i \longrightarrow \mathbf{5}$$

Theoretical hardness is then evaluated as:

$$H_v^{com} = \prod_{i=0}^{n} (H_v^{P_i})^{\frac{n_i c_i / M_i}{\sum_{i=0}^{n} n_i c_i / M_i}}$$

- i=0 shows matrix phase
- i=1,2,3…., n shows adding phase

Chapter # 3: SiAlON-SiC Composites

3.1: Introduction

Si_3N_4 and SiC are widely known for having excellent mechanical properties at high temperatures [33]. One of the major drawback of these materials is that they both are difficult to sinter [3,34]. In order to ease the process, additives are added in the liquid phase sintering method resulting in intergranular phase which offers little creep and oxidation resistance. In order to make these properties better, SiAlON-SiC composites were formed [6].

3.2: Synthesis Methods

There are many different synthesis methods for α-SiAlON-SiC composites. Some of which are:

1. $CaCO_3$ is used as a sintering additive in the formation of α-SiAlON-SiC composite. Ca-α-SiAlON achieves complete densification at even low temperature like 1600 ^oC and also used to avoid decomposing β-SiC. The precursors include Si_3N_4, AlN, $CaCO_3$. B-SiC was added from 0-40% by wt. the mixture is ultrasonically mixed and milled for 1 day in ethanol. After drying the mixture, it is placed in a steel die where it is cold pressed followed by hot pressing in graphite die. Coating of BN was used in graphite die to inhibit any reaction between die and mixture. Samples were calcined at about 1000 ^oC for roughly 1 hr, followed by heating till the sintering temperature (around 1700 ^oC) at hot pressed at 25 MPa for 1 hr. Heating rate is around 30 ^oC/min while cooling rate is around 60 ^oC/min [35].
2. Y_2O_3 is used as a sintering additive along with other rare-earth oxides. β-SiC was added in Si_3N_4-AlN-RE_2O_3 in varying concentrations from 0-20% by wt. The powder was first ball milled for about 2 hrs in ethanol followed by drying it for 12 hrs at 120 ^oC. The powder is cold compressed which is followed by 2-step gas pressured sintered for half hour in about 0.1 MPa in N_2 atmosphere at 1750 ^oC followed by heating at 1950 ^oC in 1.5 MPa in N_2 atmosphere. The heating rate is about 10 ^oC/min [36].
3. Different concentrations of SiC is mixed with Si_3N_4-AlN-RE_2O_3 powder. The mixture for planetary milled in alcohol for about 2 hrs followed by drying it for about a day at 90 ^oC. The dried powder was then compacted using cold uniaxial pressing for about half min under 30 MPa followed by the cold isostatic pressing for 1 min under 300 MPa. The resulting solution is divided into 2 groups. On one group a 2-step gas pressured sintering is performed while on the other group, hot pressure is applied under 20 MPa for half hour at 1750 ^oC [6].
4. α-SiC is varied from 0-40% by wt in composition of α-SiAlON/α-SiC composite. The sintering additive used is Y_2O_3 while the precursors are Al_2O_3, α-SiC and Si_3N_4. After suitable concentrations of the precursors, it is mixed and milled for about half a day in ethanol. Silicon nitride ball is used as a medium for this process. The powder undergoes SPS at 1800 ^oC for around 5 min with pressure of under 20 MPa. The atmosphere used is N_2 with a pressure of 0.1 MPa. The heating rate is set at 100 ^oC/min while the cooling rate is set at 200 ^oC/ min until 900 ^oC is reached [37].

5. Ca-α-SiAlON reinforced with SiC using SPS method. The precursors include α-Si3N4, SiO2, AlN and CaO2. SiC is varied from 0-30% by wt. By using ethanol as a medium, the mixture is passed through ultrasonic probe sonicator and dried for about half a day in the furnace at 80 ^{o}C. [38].

3.3: Phase Assembly and Morphology

The phase assembly and morphologies of the above performed experiments are as follows:

1. Samples having 20% SiC were taken into observation and were hot pressed for about an hour at 25 MPa. This was performed between 1400-1800 ^{o}C with and interval of 100 ^{o}C. Oxides, Silicon Nitride, and Aluminum Nitride reacts to form $2CaO\text{-}SiO_2\text{-}Al_2O_3$ which is known as Gehlinite, which after reacting 1400 ^{o}C forms into a liquid phase which absorbs Silicon Nitride and Aluminum Nitride. This results in the formation of Ca-α-SiAlON through precipitation. Precipitation is completed at around 1600 ^{o}C with no change in phase compositions. β-SiC does not go under any phase transformation also there no change in the relative intensity of the XRD test during sintering ranging of temperatures from 1400-1800 ^{o}C. Fracture surface of the samples having SiC quantity of 0%, 20% and 40% are shown below [35].

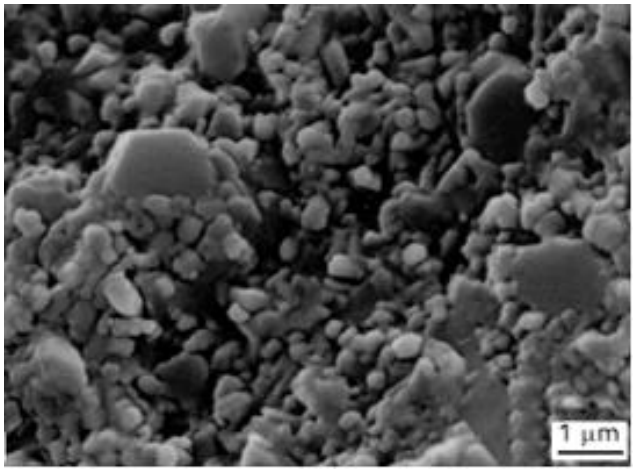

Figure 3.1: Ruptured sample having 0 wt. % SiC

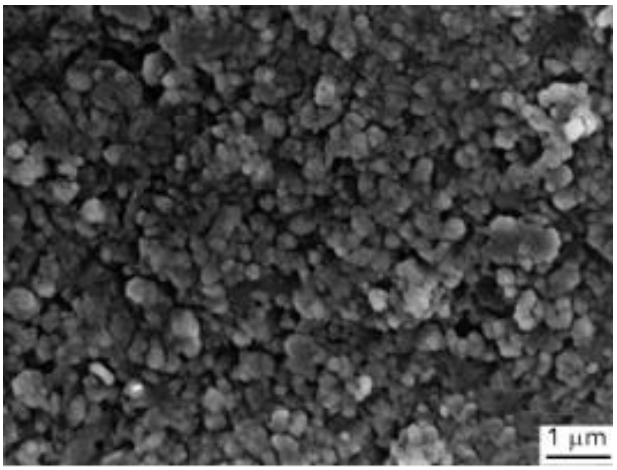

Figure 3.2: *Ruptured sample having 20 wt. % SiC*

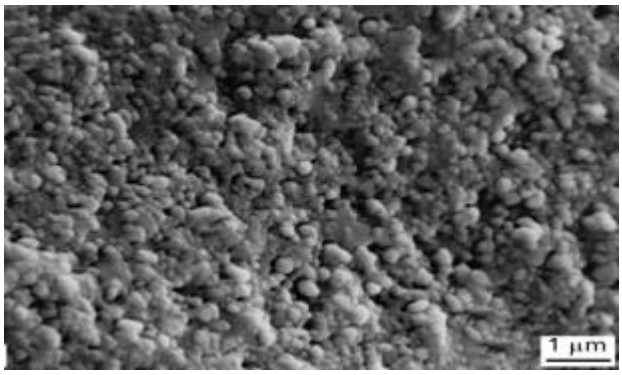

Figure 3.3*: Fracture surface of the sample with SiC 40% by wt*

By analyzing the figures, it is seen that with 0% SiC, the coarse grains have a great variability. Some grains ranges from 0.5-0.7 μm, while some even exceed 1 μm. As the amount of SiC is increased, the grain size becomes uniform and the variability decreases. The

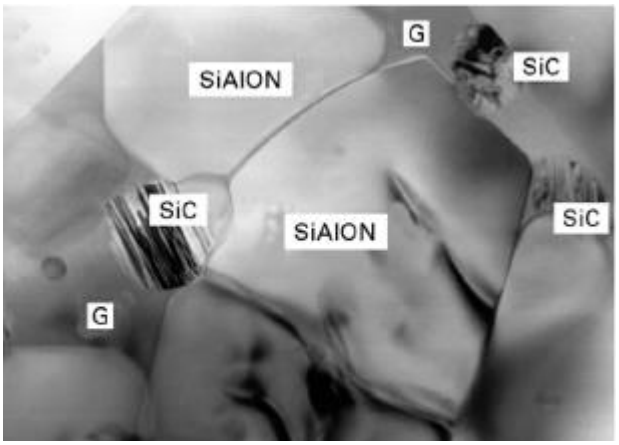

Figure 3.4: *α-SiAlON phase with SiC and amorphous phase G of sample with 20% by wt SiC prepared by hot pressing .*

resulting uniform distribution of SiC in a fine equiaxed matrix can be seen through a transmission electron micrograph which shows equiaxed polygonal alpha sialon grains with uniformly distributed SiC particles along with amorphous phase as shown below.

2. By the addition of SiC, AlN and Si_3N_4 dissolution is not affected but grain size of α-SiAlON is affected and the aspect ratio is decreased from 4.5 to 2.3. The decrease in length of the structure is observed in the below figure [36].

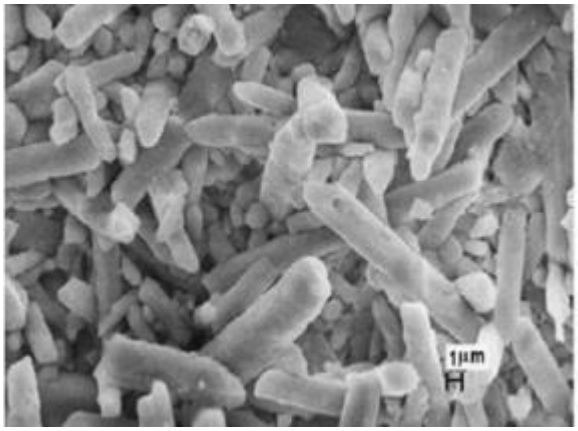

Figure 3.5: *Microstructure of the sample with SiC 0% by wt*

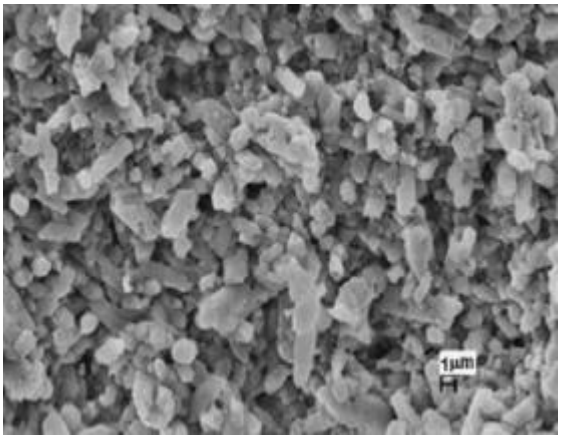

Figure 3.6: Microstructure of two-step gas pressure sintered sample with SiC 10% by wt

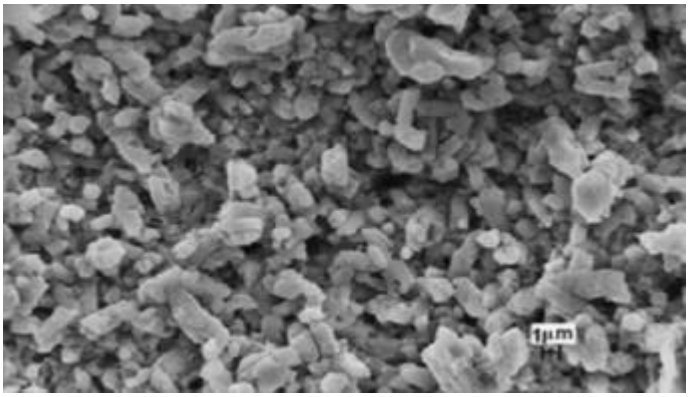

Figure 3.7: *Microstructure of sample with SiC 20% by wt*

3. XRD of the sample shows only α-SiAlON and β-SiC, which shows that there is no reaction between SiC and other precursors. Increase on %age of SiC shows decrease in the aspect ratio from about 4 to 2.5 for hot press sintering as shown in the figures below [6].

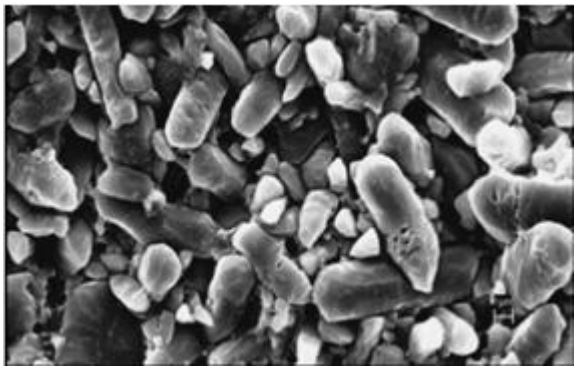

Figure 3.8: *Microstructure of hot pressed sintered sample with SiC 0% by wt*

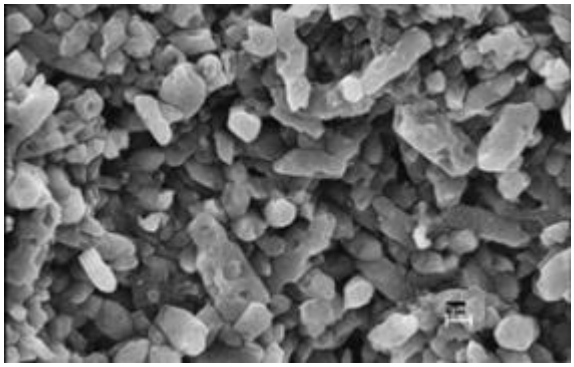

Figure 3.9*: Microstructure of hot pressed sintered sample with SiC 10% by wt*

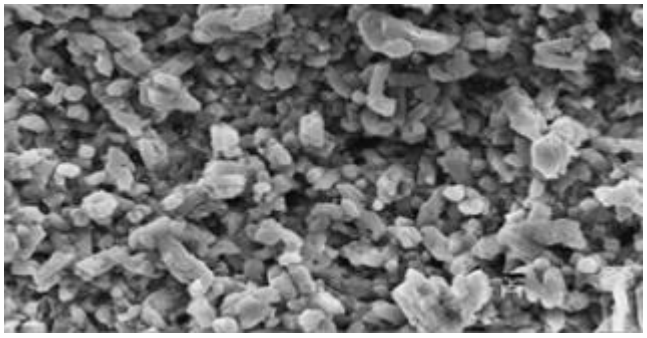

Figure 3.10*: Microstructure of hot pressed sintered sample with SiC 20% by wt*

4. α-SiAlON/α-SiC ceramic materials are formed via SPS. FESEM images of mixed powder with various concentrations of SiC are shown below. For the concentration range of SiC

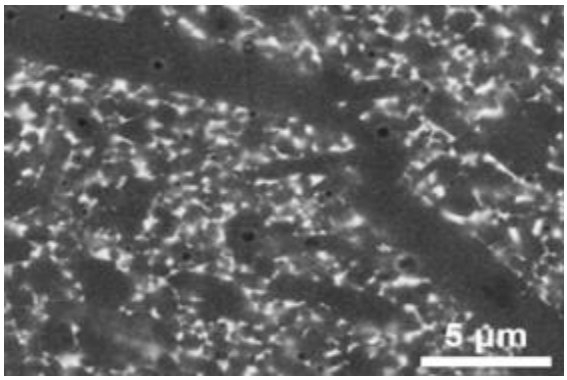

Figure 3.11*:* FESEM image of the SPS sample with SiC concentration of 0% by wt

by wt from 0-5%, the α-SiAlON grains have an average width of 2.5 µm. As the concentration is increased, α-SiAlON grains give way to smaller grains leading to equiaxed fine matrix microstructure. Anisotropic growth of SiC grains was due to Ostwald ripening rather than SiC going under any poly-type transformation with the sintering liquid from additive Y_2O_3 and the high heating rates of SPS technique aiding the anisotropic grain growth [37].

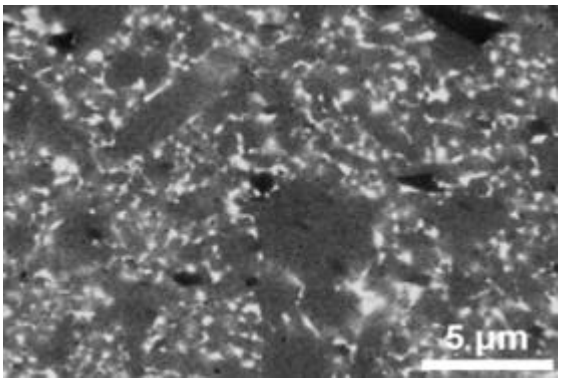

Figure 3.12: *FESEM image of the SPS sample with SiC concentration of 5% by wt*

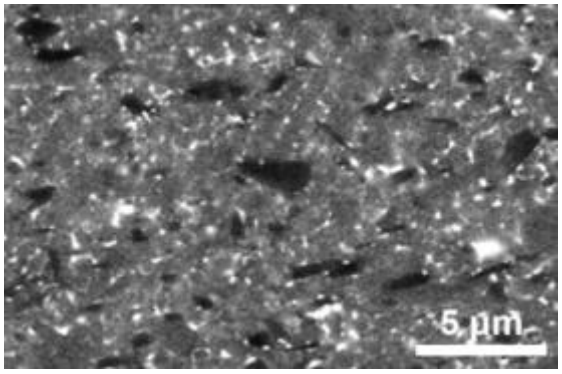

Figure 3.13*: FESEM image of the SPS sample with SiC concentration of 10% by wt*

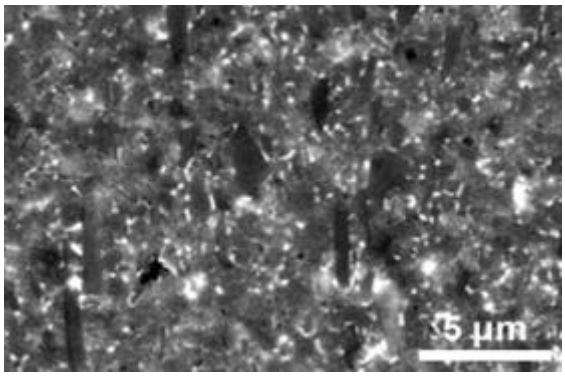

Figure 3.14*:* FESEM image of the SPS sample with SiC concentration of 20% by wt

5. The α-SiAlON/SiC ceramic formed shows the mechanism which enhances fracture toughness. In **Figure (18 a)** the fracture surface of a sample with SiC having concentration of 0% by wt can be seen having an intergranular fracture but in **Figure (18 b)** of SiC having concentration of 30% by wt the fracture surface has grain pull-outs identified by red circles. These grains could be either of SiC or of sialon. Furthermore, also in the fracture surface of sample with SiC having concentration of 30% by wt, cleavage steps are seen in **Figure (18 c).** Furthermore, another fracture toughness enhancing mechanism, crack deflection, can be seen in the micrograph of indent test carried out on sample with SiC having concentration of 30% by wt where the SiC particles can be seen deflecting the crack **Figure (19)**. Mechanisms such as grain pull-out, cleavage steps and crack deflection increase fracture toughness [38].

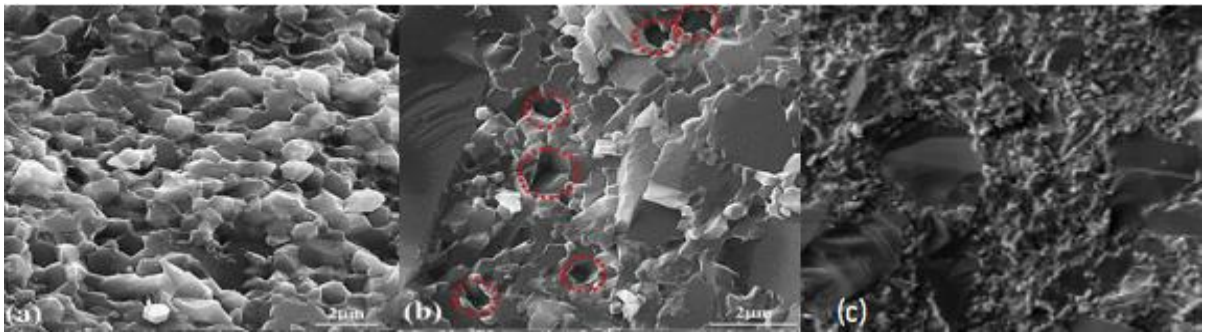

Figure 3.15*:* Fracture surface of sample with SiC concentration by wt
(a) 0% (b) 30% (c) 30%

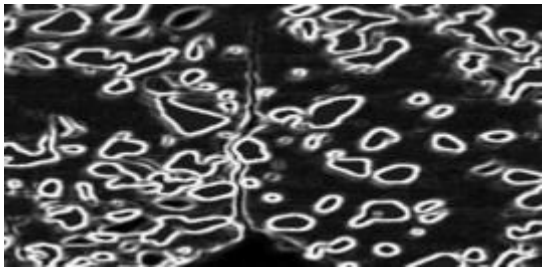

Figure 3.16: Micrograph of indentation test of alpha SiAlON-SiC composite with SiC concentration of 30% by wt

3.4: Theoretical and Actual Hardness

The theoretical hardness of α-SiAlON/SiC can be calculated by the formula:

$$H_v^{com} = \prod_{i=0}^{n} (H_v^{P_i})^{\frac{n_i c_i / M_i}{\sum_{i=0}^{n} n_i c_i / M_i}}$$

Where at 1900 ^{o}C:

- For α-SiAlON

i	0
n	48
M	594.3141
H_v^{Pi}	19.9

- For SiC

i	1
n	4
M	40.096
H_v^{Pi}	25.5

Using these values in the formula, the theoretical hardness in GPa at different concentrations are as:

Table 3-1: Theoretical hardness of α-SiAlON/SiC composites at different concentrations of SiC at 1900 ^{o}C

0% SiC	19.9
5% SiC	20.20349376
10% SiC	20.5044834
15% SiC	20.80296727
20% SiC	21.09894575
30% SiC	21.68339722
40% SiC	22.5787568

Similarly, at 1700 ^{o}C:

- For α-SiAlON

i	0
n	48
M	599.893
H_v^{Pi}	17.25

- For SiC

i	1
n	4
M	40.096
H_v^{Pi}	25.5

Using these values in the formula, the theoretical hardness in GPa at different concentrations are as:

Table 3-2: Theoretical hardness of α-SiAlON/SiC composites at different concentrations of SiC at 1700 ºC

0% SiC	17.25
5% SiC	17.67023269
10% SiC	18.09021308
15% SiC	18.509825363
20% SiC	18.92896064
30% SiC	19.765387069
40% SiC	20.59872314

The experimental hardness in GPa of the composites at different concentrations in different experiments is shown below along with % error with the theoretical hardness.

Table 3-3: Experimental hardness of experiment 1 and its difference with theoretical hardness [35]

% SiC	***Hardness (GPa)***	***% error***
0	17.25	0
10	17.74	1.93
20	18.67	1.36
30	18.7	5.39
40	19.02	7.66

Table 3-4: Experimental hardness of experiment 2 and its difference with theoretical hardness [36]

% SiC	***Hardness***	***% error***
0	18.5	0
5	18.9	0.16
10	18.2	5.39
15	15	23.47
20	12	39.9

Table 3-5: Experimental hardness of experiment 3 and its difference with theoretical hardness [6]

% SiC	***Hardness***	***% error***
0	20.1	0
5	20.4	0.01
10	20.9	1
15	21.1	0.56
20	21.4	0.61

Table 3-6: Experimental hardness of experiment 4 and its difference with theoretical hardness [37]

% SiC	***Hardness***	***% error***
0	19.9	0
5	20.7	2.4
20	21.6	2.32
40	22.8	2.37

Table 3-7: Experimental hardness of experiment 5 and its difference with theoretical hardness [38]

% SiC	***Hardness***	***% error***
0	21.1	0
10	21.5	0.4
20	23.1	4.48
30	24.5	8.04

Chapter # 4: SiAlON-ZrN Composites

4.1: Introduction

Zirconium Nitride (ZrN) has a wide variety of uses in industries [39-42]. The main reason for its uses are due to its excellent thermal and chemical stabilities [43]. At room temperature, it has an electrical resistivity of 12.0 μ Ω cm [44]. SiAlON-ZrN composites combines the advantages of both materials providing excellent performance like high fracture toughness [45], good thermal shock resistance, high-temperature corrosion resistance [46] and wear resistance. β-SiAlON is the steadiest among SiAlON family [47,48]. General form of β-SiAlON is [49]:

$$Si_{6-z}\text{-}Al_z\text{-}O_z\text{-}N_{8-z}$$ **(where z varies from 0 to 4.2)**

4.2: Synthesis Methods

The different methods for the synthesis of β-SiAlON-ZrN ceramics are as follows:

1. ZrN-coated Si_3N_4 is sintered along with additives like AlN, Y_2O_3 and Al_2O_3 at N_2 atmosphere for 2 hrs at 1850 ^oC. consider this sample as A1. Now consider another sample A2, in N_2 atmosphere at 1600 ^oC, ZrN-coated Si_3N_4 was calcined for about 2 hrs. After this process, using same additives and process the powder is sintered [40].
2. ZrN is varied from 0-50% by wt in β-SiAlON (z=1). Sintering additive used was YAG composition (Y_2O_3 and Al_2O_3 with a molar ratio of 3:5 or $Y_3Al_5O_{12}$). Powder is ball-milled for about 4 hrs in iso-propanol and dried in a rotary evaporator. Sample was nitrided in a graphite furnace under 0.4 MPa pressure of high-purity nitrogen gas for 3 hours at a temperature of 1400 °C [47].
3. β-SiAlON (z=4) and ZrN are used. The powders are cold pressed at 200 MPa. The green pellets are sintered at 1600 °C and 1700 °C under a N_2 atmosphere for 4 hours. [50].

4.3: Phase Assembly and Morphology

Phase assembly and morphologies of the above experiments is as follows:

1. β-SiAlON grains are surrounded by ZrN grains in sample A1 as shown in the figure below. ZrN grain size ranges from 1-1.5 μm. Due to zirconia grains, transient liquid phase was observed in β-SiAlON particles. The morphology of the ZrN grains was round and irregular while that of β-SiAlON grains was prismatic and faceted.

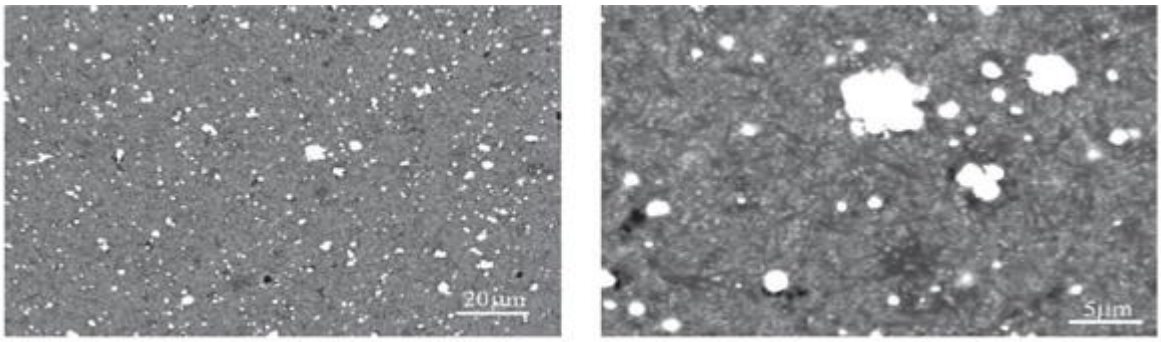

Figure 4.1: *Electron Micrograph of sample A1*

In sample A2, brighter ZrN particles could be observed in between the darker, elongated β-SiAlON particles. The ZrN particles, having irregular shape, were distributed in a non-homogeneous pattern, but had the same size as in sample A1. It is clear that the transient liquid phase was in between the β-SiAlON particles. The problem with both these phase assemblies was the same; that it caused little electrical conductivity. The reason was that the conductive ZrN phase was surrounded by the β-SiAlON particles, consequently blocking its electrical conductivity characteristics. The ZrN particles were farther from each other too, which only increased the electrical resistivity [40].

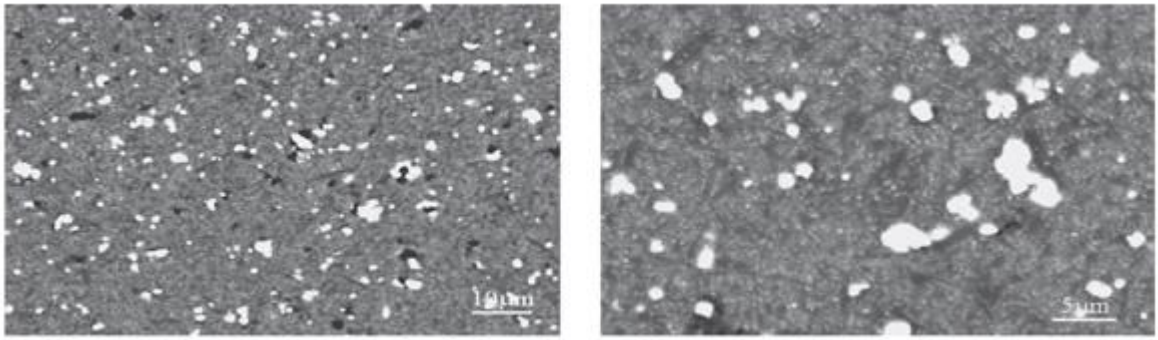

Figure 4.2: Electron Micrograph of sample A2

2. β-SiAlON (z=1) had an elongated morphology. ZrN was varied from 0-50% by wt. ZrN and β-SiAlON (z=1) were sintered at 1600 °C, with an intermediate phase of YAG

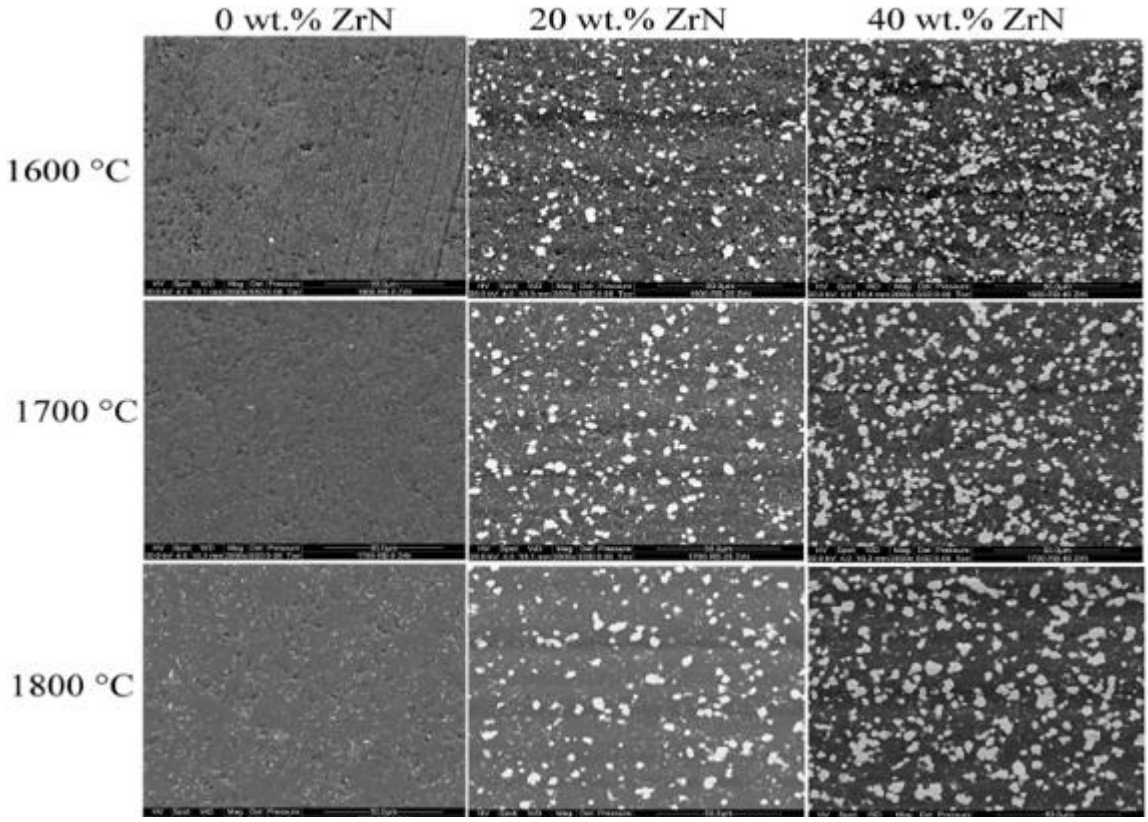

Figure 4.3: *Composites sintered at different temperatures with different content of ZrN*

($Y_3Al_5O_{12}$). Similarly, at 1700 ºC sintered composites were ZrN, β-SiAlON (z=1) and intermediate phase of $Y_5Si_4Al_2O_{17}N$. The various ZrN contents had no effect on the phase assemblage for these sintering temperatures. Increasing ZrN to 20% by wt, β-SiAlON (z=1) disappeared completely and was changed into Y-α-SiAlON (β to α phase transformation). The intermediate phases were $Y_2Si_3O_3N_4$ at 20% by wt and 30% by wt of ZrN; and 21R-Sialon ($SiAl_6O_2N_6$) for 40% by wt and 50% by wt of ZrN [47]. The morphologies at different temperatures and concentrations is shown below along with the phase assembly table:

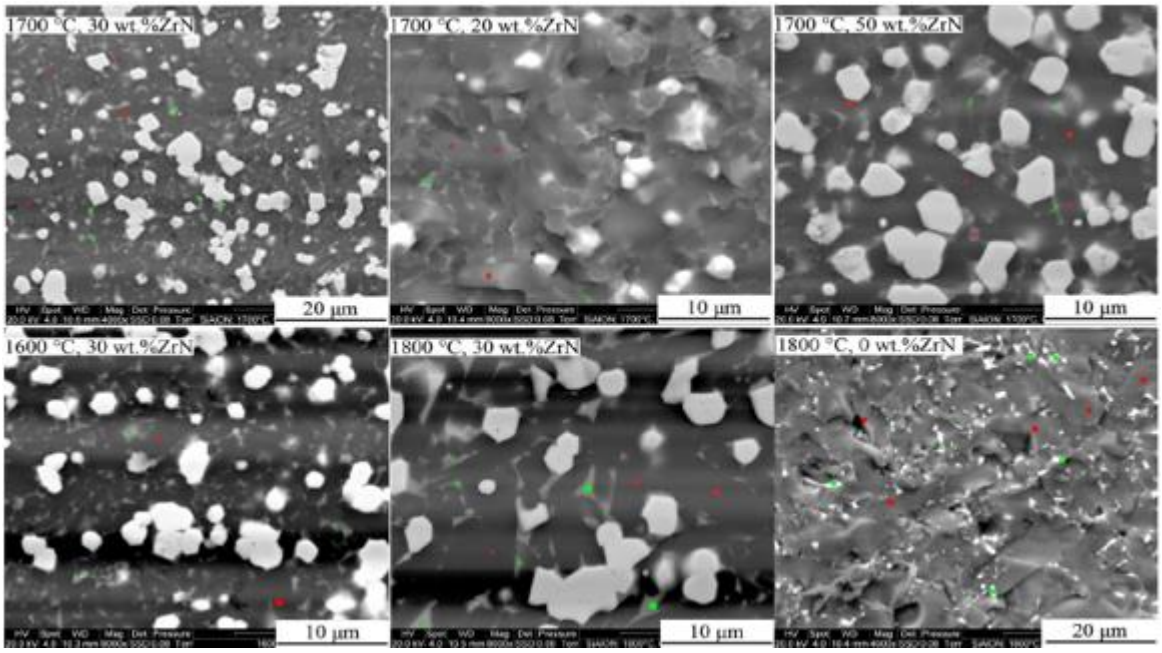

Figure 4.4: *High magnification of Figure 22. Red dot represents β-SiAlON grains while green represents intermediate phase*

Table 4-1: Phases of the samples prepared at 1600 and 1700°C (β-SiAlON (z = 1)) [47]

	T = 1600 °C	**T = 1700 °C**

ZrN content (wt %)	Phases		Phases	
	Major	*Intermediate*	*Major*	*Intermediate*
0	β-SiAlON (z=1)	$Y_3Al_5O_{12}$	β-SiAlON (z=1)	$Y_5Si_4Al_2O_{17}N$
10 - 50	β-SiAlON (z=1) ZrN		β-SiAlON (z=1) ZrN	

3. Sintering temperatures were 1600 and 1700 ºC and variation of ZrN was from 0-50% by wt. The phase assembly is shown in the table below. At 1600 °C, the composition of the composites was β-SiAlON (z = 4) with ZrN having concentration of 0% by wt; ZrN and β-SiAlON (z = 4) at ZrN having concentration of 10–50% by wt as the main phases. Meanwhile the intermediate phases consisted of AlN-Polytype SiAlON, $ZrAl_3O_3N$, $Zr_{0.82}Y_{0.18}O_{1.91}$, $Y_3Al_5O_{12}$ and Al_2O_3 all of which depended on the ZrN content. At 1700 °C, the major phases were β-SiAlON (z = 4) and 15R-SiAlON without ZrN content; β-SiAlON (z = 4), 15R-SiAlON and ZrN with ZrN having concentration of 10 – 50% by wt. For the sample without ZrN, a new intermediate phase Y_4SiAlO_8N was seen and with increasing ZrN content, a new intermediate phase ($SiAl_5O_2N_5$ aka 12H-Sialon) appeared [50]. The morphologies are shown in below:

Table 4-2: Phase of samples prepared at 1600 and 1700 ºC (β-SiAlON (z = 4)) [50]

ZrN content (wt %)	T = 1600 °C Phases		T = 1700 °C Phases	
	Major	*Intermediate*	*Major*	*Intermediate*
0	B-SiAlON (z=4)	15R-SiAlON 21R-SiAlON	β-SiAlON (z=4) 15R-SiAlON	$ZrAl_3O_3N$ Y_4SiAlO_8N
10 - 50	β-SiAlON (z=4) ZrN	$ZrAl_3O_3N$ $Zr_{0.82}Y_{0.18}O_{1.91}$ $Y_3Al_5O_{12}$ Al_2O_3	β-SiAlON (z=4) ZrN 15R-SiAlON	$Zr_{0.82}Y_{0.18}O_{1.91}$ Al_2O_3 12H-SiAlON

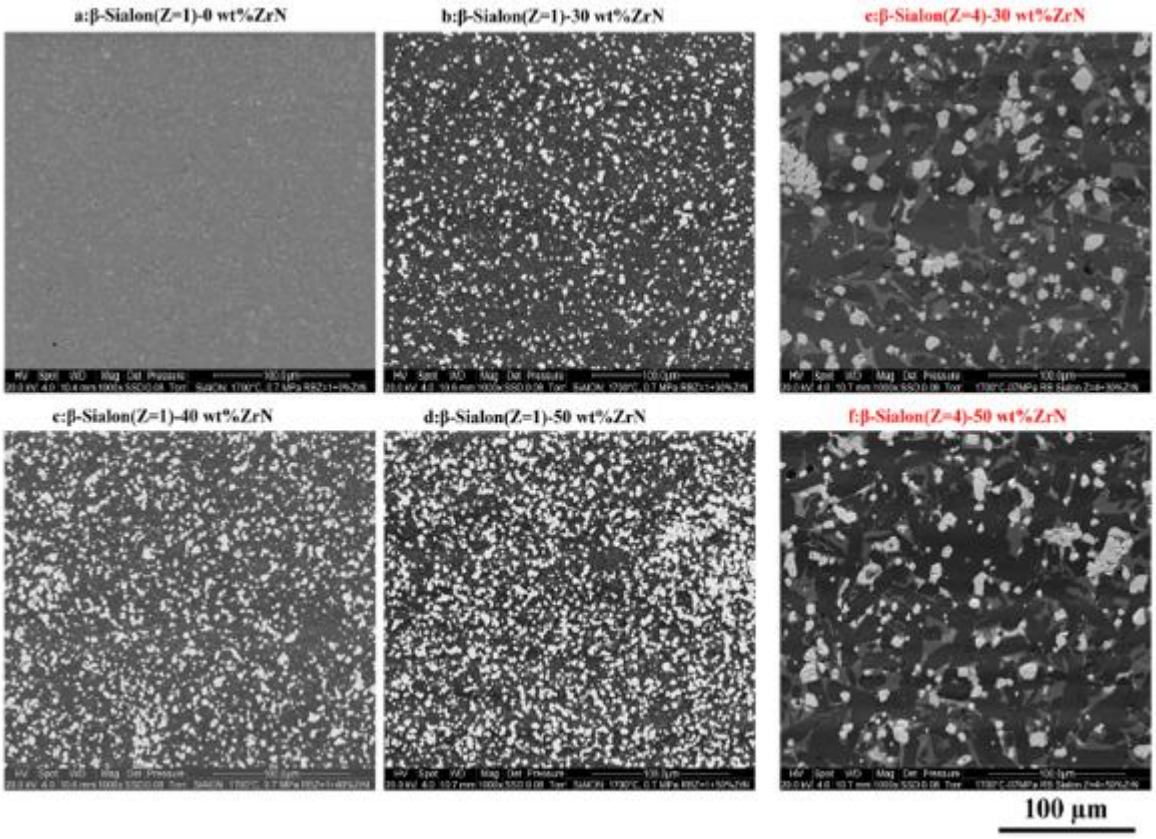

Figure 4.5: *Dispersal of ZrN in the samples formed at 1700 ^{o}C*

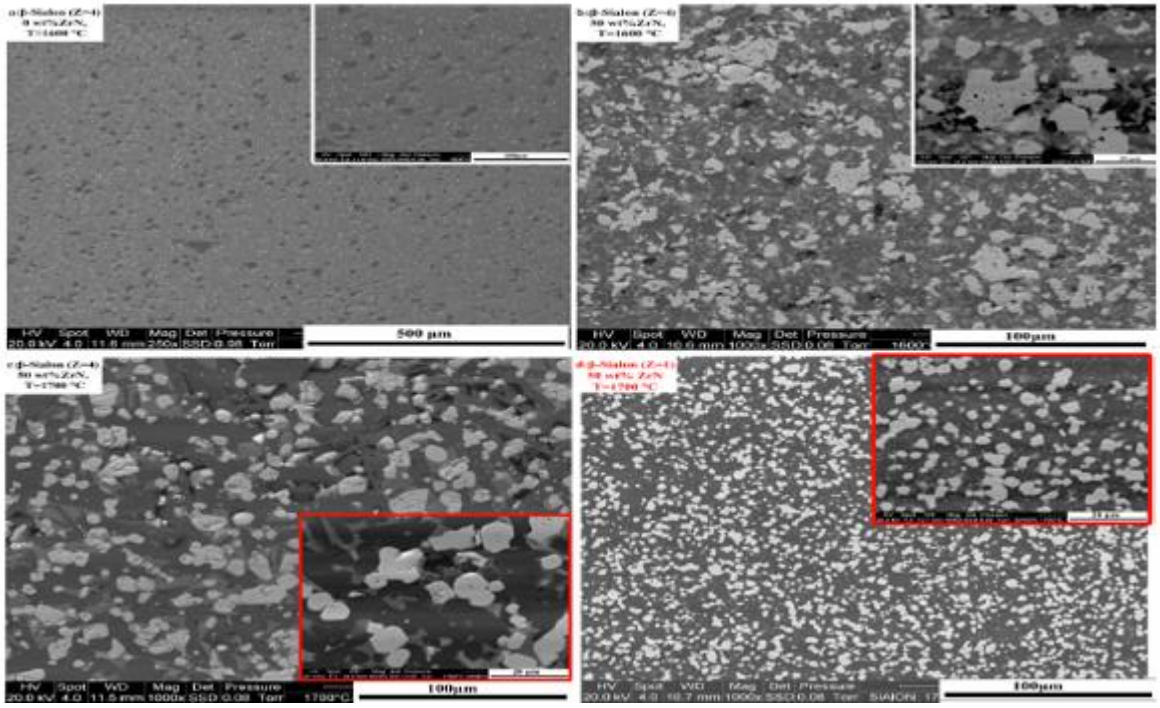

Figure 4.6: Morphological comparison of different samples of ZrN-SiAlON (a) β-SiAlON with z=4 having ZrN concentration of 0% by wt prepared at temperature 1600 °C; (b) β-SiAlON with z=4 having ZrN concentration of 50% by wt prepared at temperature 1600 °C; (c) β-SiAlON with z=4 having ZrN concentration of 50% by wt prepared at temperature 1700 °C; and (d) β-SiAlON with z=1 having ZrN concentration of 0% by wt prepared at temperature 1700 °C

4.4: Theoretical and Actual Hardness

The formula for theoretical hardness is given as:

$$H_v^{com} = \prod_{i=0}^{n} (H_v^{P_i})^{\frac{n_i c_i / M_i}{\sum_{i=0}^{n} n_i c_i / M_i}}$$

- ***z=1***

For temperature at 1600 ^{o}C:

- For β-SiAlON

i	0
n	23
M	281.46
H_v^{Pi}	14.84

- For ZrN

i	1
n	3
M	40.096
H_v^{Pi}	22.7

Using these values in the formula, the theoretical hardness in GPa at different concentrations are as:

Table 4-3: Theoretical Hardness of β-SiAlON/ZrN Composite (z=1) at 1600 ^oC

0% ZrN	14.84
10% ZrN	14.43402209
20% ZrN	16.06264175
30% ZrN	16.72842562
40% ZrN	17.43416988
50% ZrN	18.18292424

Similarly, for temperature 1700 ^oC

- For β-SiAlON

i	0
n	23
M	281.46
H_v^{Pi}	15.25

- For ZrN

i	1
n	3
M	40.096
H_v^{Pi}	22.7

Using these values in the formula, the theoretical hardness in GPa at different concentrations are as:

Table 4-4: Theoretical Hardness of β-SiAlON/ZrN Composite (z=1) at 1700 ^oC

0% ZrN	15.25
10% ZrN	15.82057011
20% ZrN	16.4228411
30% ZrN	15.05907354
40% ZrN	17.73172322
50% ZrN	18.44346093

- ***z=4***

For temperature at 1600 ^oC:

- For β-SiAlON

i	0
n	20
M	284.12
H_v^{Pi}	6.27

- For ZrN

i	1
n	3
M	40.096
H_v^{Pi}	22.7

Using these values in the formula, the theoretical hardness in GPa at different concentrations are as:

Table 4-5: Theoretical Hardness of β-SiAlON/ZrN Composite (z=4) at 1600 ^oC

0% ZrN	6.27
10% ZrN	7.18268274
20% ZrN	8.214338614
30% ZrN	9.378618558
40% ZrN	10.69057188
50% ZrN	12.16648539

Similarly, for temperature 1700 ^oC

- For β-SiAlON

i	0
n	20
M	284.12
H_v^{Pi}	10.2

- For ZrN

i	1
n	3
M	40.096
H_v^{Pi}	22.7

Using these values in the formula, the theoretical hardness in GPa at different concentrations are as:

Table 4-6: Theoretical Hardness of β-SiAlON/ZrN Composite (z=1) at 1700 ^oC

0% ZrN	10.2
10% ZrN	11.09934099
20% ZrN	12.06530513
30% ZrN	13.10183008
40% ZrN	14.21302072
50% ZrN	15.40315282

The experimental hardness in GPa of the composites at different concentrations in different experiments is shown below along with % error with the theoretical hardness.

Table 4-7: Experimental hardness of β-SiAlON-ZrN composite with z=1 at 1600 ºC with % error from the theoretical values [40]

% ZrN	***Hardness (GPa)***	***% error***
0	14.84	0
10	15.23	1.93
20	14.84	7.61
30	14.52	13.2
40	14.16	18.78
50	13.22	27.3

Table 4-8: Experimental hardness of β-SiAlON-ZrN composite with z=1 at 1700 ºC with % error from the theoretical value [47]

% ZrN	***Hardness (GPa)***	***% error***
0	15.25	0
10	15.69	0.82
20	16.05	2.27
30	15.38	9.84
40	14.96	15.63
50	14.41	21.86

Table 4-9: Experimental hardness of β-SiAlON-ZrN composite with z=4 at 1600 ºC with % error from the theoretical value [50]

% ZrN	***Hardness (GPa)***	***% error***
0	6.27	0
10	11.06	35
20	10.49	21.7
30	10.92	14.1
40	10.12	5.63
50	9.95	22.27

Table 4-10: Experimental hardness of β-SiAlON-ZrN composite with z=4 at 1700 oC with % error from the theoretical value [50]

% ZrN	***Hardness (GPa)***	***% error***
0	-	-
10	11.96	7.2
20	12.86	6.18
30	12.39	5.75
40	10.94	29.9
50	11.11	38.64

Chapter # 5: SiAlON-WC Composites

5.1: Introduction

Some of the noteworthy properties of Tungsten Carbide (WC) include high hardness, flexural strength and melting point, low friction coefficient and excellent corrosion resistance [51-64]. By reinforcing SiAlONs with WC, the hardness of the composite is increased. The common matrix phase used can be either α-SiAlON or β-SiAlON or α-β-SiAlON composition [65-67]. Sometimes WC can also be used as a matrix phase while SiAlON as secondary phase. α-SiAlON provides high hardness while β-SiAlON provides high toughness. Main method used for preparation of this composite is Spark Plasma Sintering (SPS) technique [68-70].

5.2: Synthesis Methods

There are many methods for SiAlON-WC composites. Some of which are:

1. Si_3N_4, AlN, Y_2O_3 and Al_2O_3 is mixed in acetone medium for about 6 hrs. The powder is collected after being dried. The powder is mixed with WC in the same medium for about 3 hrs. α-SiAlON is mixed with WC in different proportions in 20%, 30% and 40% by wt. The powder is then sintered for about 25 min in 40 MPa pressure at 1750 ^oC [71].
2. WC is used as a matrix phase while β-SiAlON having concentration ranging from 20-40% by wt is used a secondary phase. Consolidation of the mixture consisting of AlN, Y_2O_3, Si_3N_4 and Al_2O_3 is performed in SPS furnace for about 25-30 min under 40 MPa pressure at 1750 ^oC [72].
3. α-SiAlON is used a matrix phase while WC is used as a secondary phase. While using acetone as a medium, mixture of AlN, Y_2O_3, Si_3N_4 and Al_2O_3 is mixed for about 6 hrs in agate pestle and mortar by hand. The powder followed by WC having different concentrations ranging from 20-40% by wt is mixed again for 3 hrs. It is the consolidated using Spark plasma sintering for 25 min in 40 MPa pressure at 1750 ^oC [73].

5.3: Phase Assembly and Morphology

The phase assembly and the morphologies of the above mentioned experiments are as follows:

1. The grain structure of pure WC and α-SiAlON-WC composite along with the grain distribution of α-SiAlON and WC is shown in the figure below.

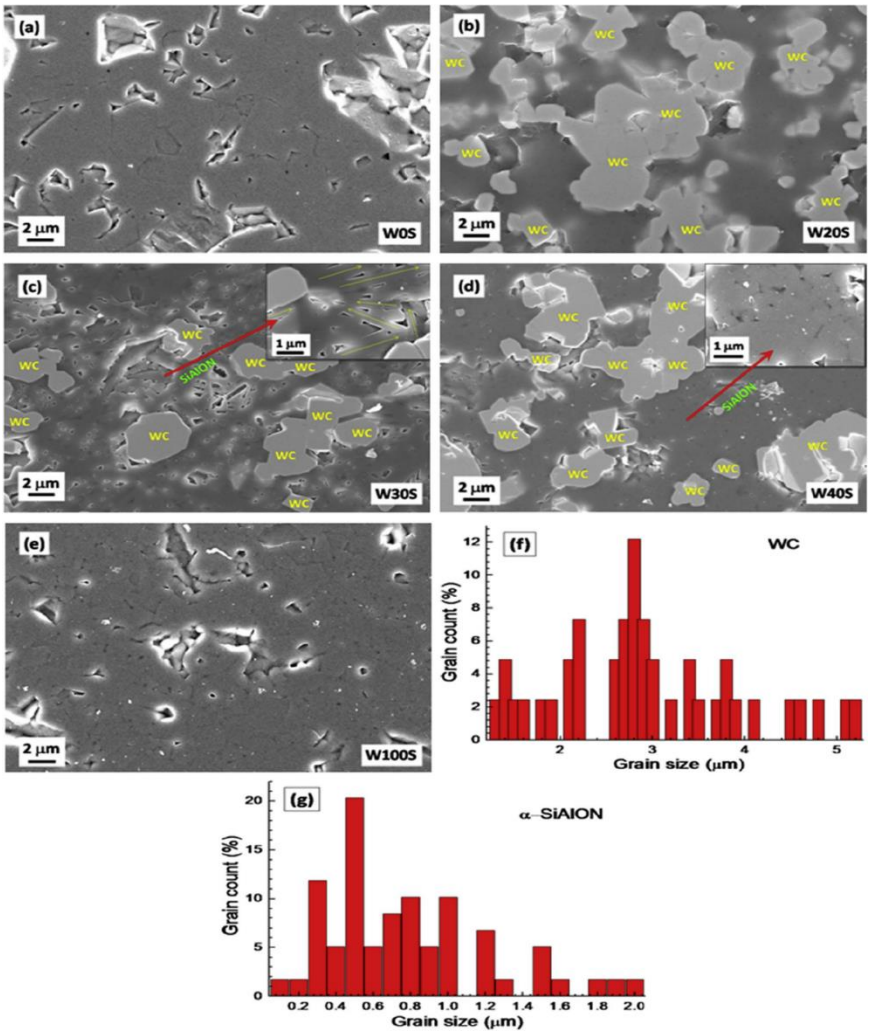

***Figure 5.1*:** Microstructure of (a) Pure WC (b) 20% by wt α-SiAlON (c) 30% by wt α-SiAlON (d) 40% by wt α-SiAlON (e) Pure α-SiAlON
Grain size distribution of (f) WC (g) α-SiAlON

The table showing different concentrations of α-SiAlON in WC and their representation/sample ID is shown in the table below:

Table 5-1: Sample ID of different composition of α-SiAlON in WC

Composition	***Sample ID***
100% WC	W0S
80% WC + 20% α-SiAlON	W20S
70% WC + 30% α-SiAlON	W30S

60 % WC + 40% α-SiAlON	W40S
100% α-SiAlON	W100S

In pure WC structure, WC grains are equiaxed with few closed pores at grain junction. In 20% α-SiAlON-WC (W20S) composite, both grains are almost identical to each other, the reason being the low density of α-SiAlON which results in similar volume fraction. In W30S, the formation of α-SiAlON grains in elongated, and WC grains forms an electrical percolating network of matrix grains. Elongation of α-SiAlON grains results in the increase in fluidity of the grain boundary liquid phase. In W40S, α-SiAlON grains were noticed to be equiaxed and sub-micron sized. W100S contains dense α-SiAlON grains [71].

2. The table showing different concentrations of β-SiAlON in WC and their representation/sample ID is shown in the table below:

Table 5-2: Sample ID of different composition of β-SiAlON in WC

Composition	***Sample ID***
100% WC	W0β
80% WC + 20% β-SiAlON	W20β
70% WC + 30% β-SiAlON	W30β
60 % WC + 40% β-SiAlON	W40β
100% β-SiAlON	W100β

The grain morphology of pure WC, W30β and pure β-SiAlON is shown in the figure below.

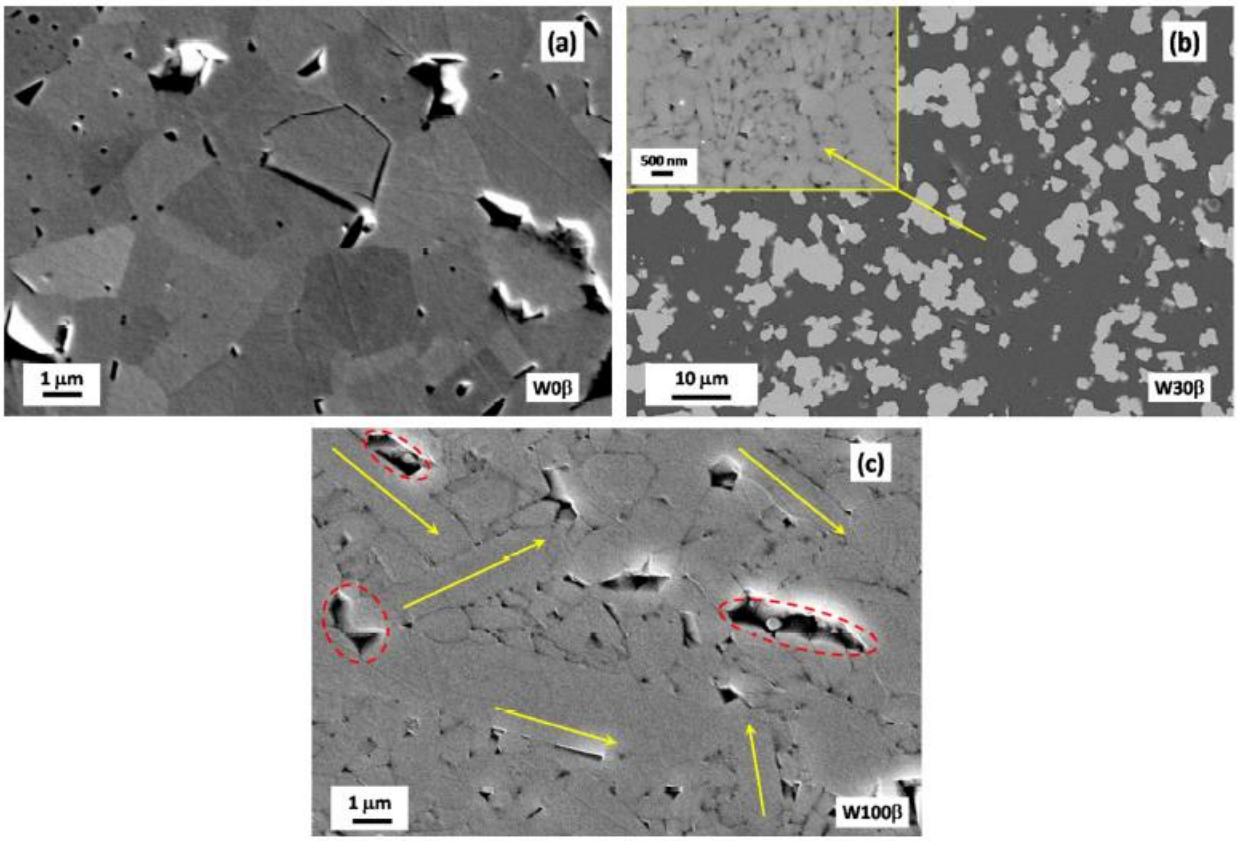

Figure 5.2: *Microstructure of (a) Pure WC (b) 30% β-SiAlON-WC Composite (c) Pure β-SiAlON*

In pure WC, the grains were noted to be in the range of 2-5 µm, with closed pores at triple grain junctions. In the structure containing β-SiAlON 30% by wt, it is uniformly divided in the WC structure. The grain morphology of β-SiAlON is fine with closed pores having dimensions between 0.05-0.25 µm. Pure β-SiAlON structure is found to be dense due to the elongated β-SiAlON grains. Some grain pull-out regions were also observed in the structure as marked in the figure above. The size of the grains is about 125 µm [72].

3. The table showing different concentrations of WC in α-SiAlON and their representation/sample ID is shown in the table below:

Table 5-3: Sample ID of different composition of WC in α-SiAlON

Composition	***Sample ID***
100% α-SiAlON	S0W
80% α-SiAlON + 20% WC	S20W
70% α-SiAlON + 30% WC	S30W
60 % α-SiAlON + 40% WC	S40W
100% WC	S100W

The structure of pure α-SiAlON and WC along with the microstructure of WC in α-SiAlON is shown below.

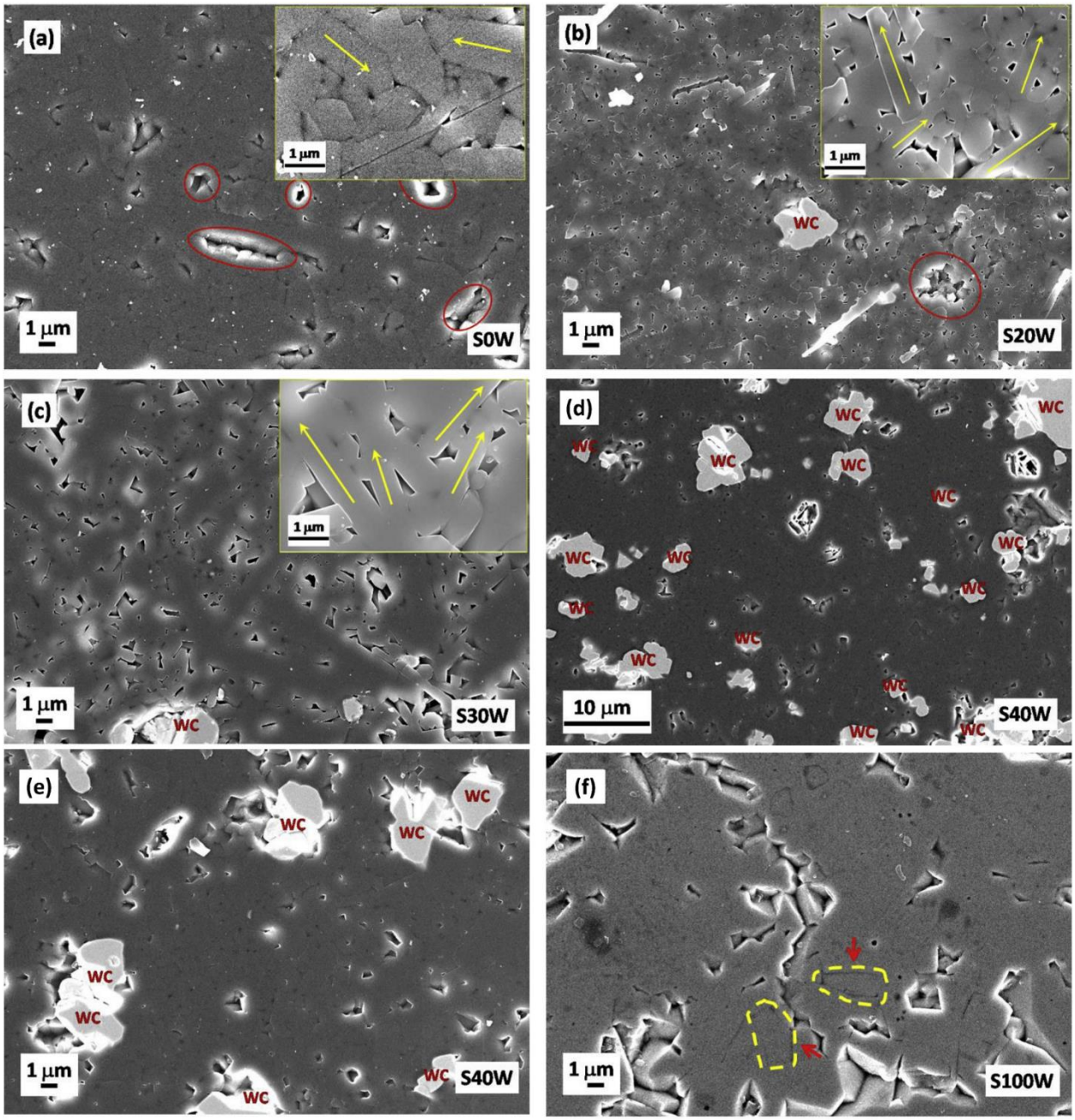

Figure 5.3: *Electron microscopy of (a) Pure α-SiAlON (b) 20% WC-α-SiAlON (c) 30% WC-α-SiAlON (d) Low magnification field emission scanning electron microscopy image of the 40 wt% WC-α-SiAlON. High magnification of microscopy of (e) 40% WC-α-SiAlON (f) Pure WC*

The structure of pure α-SiAlON is dense with certain areas containing grain pull-outs. These are formed during grinding operations in order to create fresh surface before polishing. The grain size is about 1-2 µm. In 20% WC-α-SiAlON and 30% WC-α-SiAlON,

elongation of grains is observed. These elongations help in increase the toughness of the composites. As the concentration of WC reaches about 40% by wt, WC grains becomes larger to about 2-3 μm. Pure WC structure is dense having its grain size to about 2-5 μm [73].

5.4: Theoretical and Actual hardness

The formula for the theoretical hardness of a composite is as follows:

$$H_v^{com} = \prod_{i=0}^{n} (H_v^{Pi})^{\frac{n_i c_i / M_i}{\sum_{i=0}^{n} n_i c_i / M_i}}$$

For Experiment 1:

- For WC

i	0
n	4
M	195.85
H_v^{Pi}	16.8

- For α-SiAlON

i	1
n	48
M	591.887
H_v^{Pi}	19.4

Using these values in the formula, the theoretical hardness in GPa at different concentrations are as:

Table 5-4: Theoretical hardness of different composition of α-SiAlON in WC

W0S	16.8
W10S	17.5565818
W20S	18.04847898
W30S	18.39378695
W40S	18.64949274
W100S	19.4

For Experiment 2:

- For WC

i	0
n	4
M	195.85

H_v^{Pi}	17

- For β-SiAlON

i	1
n	23
M	281.46
H_v^{Pi}	16.8

Using these values in the formula, the theoretical hardness in GPa at different concentrations are as:

Table 5-5: Theoretical Hardness of different composition of β-SiAlON in WC

W0β	17
W10β	16.9381979
W20β	16.89969093
W30β	16.87339671
W40β	16.85430048
W100β	16.8

For Experiment 3:

- For α-SiAlON

i	0
n	48
M	591.887
H_v^{Pi}	19.4

- For ZrN

i	1
n	4
M	195.85
H_v^{Pi}	16.6

Using these values in the formula, the theoretical hardness in GPa at different concentrations are as:

Table 5-6: Theoretical Hardness of different composition of WC in α-SiAlON

S0W	19.4
S10W	19.31786071
S20W	19.22171347
S30W	19.10764161
S40W	18.97012046
S100W	16.6

The experimental hardness in GPa of the composites at different concentrations in different experiments is shown below along with % error with the theoretical hardness.

Table 5-7: Experimental Hardness of α-SiAlON doped WC with % error from the theoretical hardness [71]

	Hardness (GPa)	***% error***
W0S	16.8	0
W10S	18	2.52
W20S	19.6	8.6
W30S	20	8.73
W40S	21.6	15.82
W100S	19.4	0

Table 5-8: Experimental Hardness of β-SiAlON doped WC with error from the theoretical hardness [72]

	Hardness (GPa)	***% error***
W0β	17	0
W10β	17.2	1.55
W20β	17.6	4.14
W30β	18	6.68
W40β	17.5	3.83
W100β	16.8	0

Table 5-9: Experimental Hardness of WC doped α-SiAlON with error from the theoretical hardness [73]

	Hardness (GPa)	***% error***
S0W	19.4	0
S10W	20	3.53
S20W	17.6	8.43
S30W	13.5	29.35
S40W	19.8	4.37
S100W	16.6	0

Chapter # 6: SiAlON-TiN Composites

6.1: Introduction

Composite materials increase toughness and hardness by reinforcing them with other ceramics. By reinforcing TiN in SiAlONs increases different properties and makes it easy for different uses [74-80]. At high temperatures, SiAlONs have some little inferior properties but by reinforcing TiN with them, these properties are enhanced several times [81-85]. TiN can be reinforced in either α-SiAlON, β-SiAlON or the combination of the two. SiAlON is used as a matrix phase while TiN is mostly used as a secondary phase. α-SiAlON provides high hardness while β-SiAlON provides high toughness [86]. By varying the concentrations of α-SiAlON, β-SiAlON and TiN different results are obtained.

6.2: Synthesis Method

SiAlON-TiN composites is made by varying different concentrations of α-SiAlON and β-SiAlON like α:β=10:90, 35:65 and 75:25 while also varying concentration of TiN like 17% and 25% by wt. In order to obtain the desired composition, isopropyl alcohol is used as a medium and planetary milling is done at speed of 300 rpm for 1.5 hrs using Si_3N_4 balls. TiN is added in the SiAlON mixture powder and added homogenously. Rotary evaporator is used to dry the slurries produced and the powder were dry sieved. The powder formed is pressed at about 25 MPa followed by cold isostatically pressed at 300 MPa. Two-step sintering is carried out in the final step. Pre-sintering is done for about 1 hr at 0.5 MPa at 1890 ^oC followed by second step of sintering is done in N_2 atmosphere at 2.2 MPa pressure for about an hr at 1940 ^oC. the cooling rate is set at 5 ^oC/min [87].

6.3: Phase Assembly and Morphology

The table showing different concentrations of TiN, α-SiAlON and β-SiAlON and their representation/Sample ID is shown below:

Table 6-1: Sample ID of different concentrations of TiN and α-SiAlON and β-SiAlON

Sample ID	***% TiN***	**α:β in SiAlON mixture**
T0035	0	35:65
T1735	17	35:65
T2510	25	10:90
T2575	25	75:25

The microstructure of these samples is shown in the figures below:

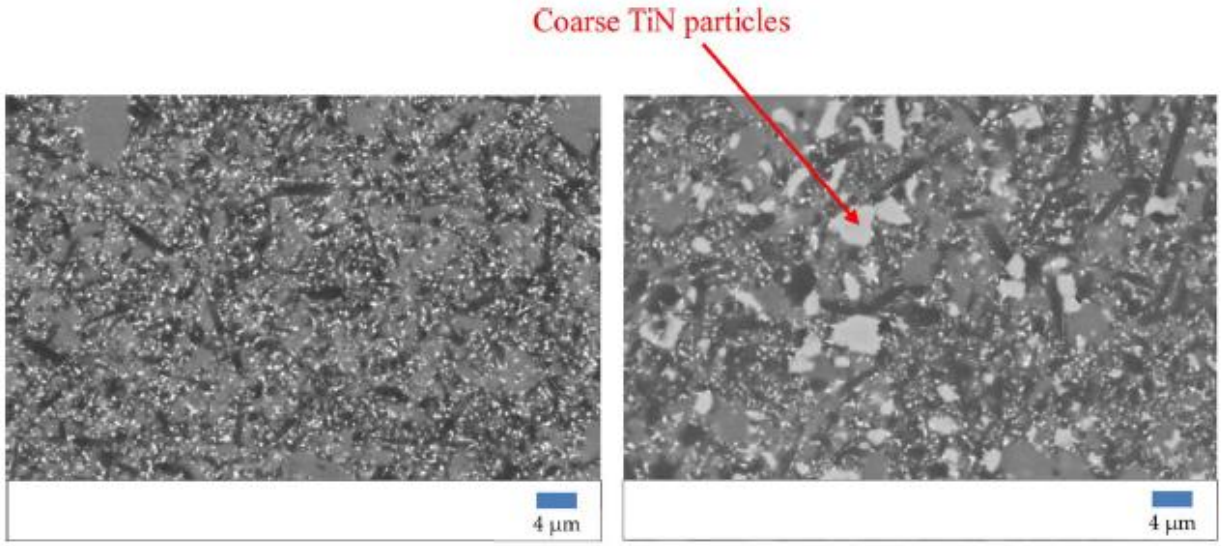

(a) (b)

Figure 6.1: Microstructure of (a) T0035 (b) T1735

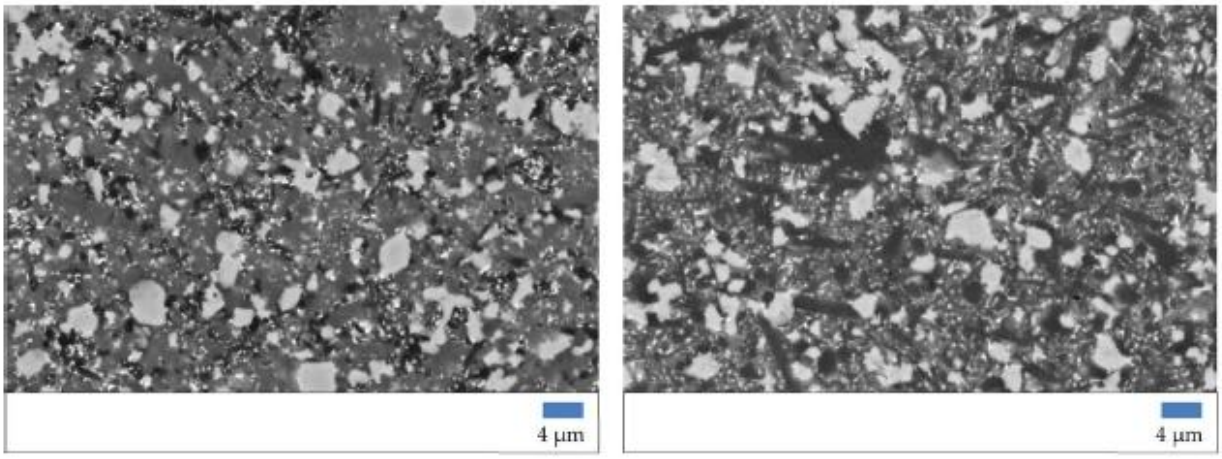

(a) (b)

Figure 6.2: *Microstructure of (a) T2575 (b) T2510*

Addition of TiN particles increases surface roughness many times. TiN helps in increasing the hardness of the composite. TiN allows lowers the Co-efficient of friction of the composite. By increasing the β-SiAlON concentration in the composite, the hardness of the composite is decreased dramatically. TiN in the composite is mixed homogenously throughout the structure.

The elongated grains formed helps in increase the fracture toughness of the overall composite. Increase in α-SiAlON also leads in increase in the Co-efficient of friction of the composite [87].

6.4: Theoretical and Experimental Hardness

The formula for theoretical hardness of a composite is as follows:

$$H_v^{com} = \prod_{i=0}^{n} (H_v^{P_i})^{\frac{n_i c_i / M_i}{\sum_{i=0}^{n} n_i c_i / M_i}}$$

- For α-SiAlON

i	0
n	48
M	591.887
H_v^{Pi}	18

- For β-SiAlON

i	1
n	23
M	281.46
H_v^{Pi}	15

- For TiN

i	2
n	3
M	61.874
H_v^{Pi}	27

The theoretical hardness of these samples are shown below:

Table 6-2: Theoretical hardness of TiN-SiAlON composite with different concentrations

T0035	15.98334276
T1735	16.91994726
T2510	16.78161088
T2575	18.53029027

The experimental hardness in GPa of the composites at different concentrations in different experiments is shown below along with % error with the theoretical hardness.

Table 6-3: Experimental Hardness of TiN doped SiAlON with error from the theoretical hardness [87]

	Hardness (GPa)	***% error***
T0035	15.73	1.58
T1735	15.87	6.2
T2510	15.9	5.25
T2575	16.57	10.58

Chapter # 7: Conclusion

In above mentioned experiments, there is seen that from low concentration in doping, the theoretical hardness calculated is nearly equal to the actual hardness of the composite. As the concentration increases, the % error also increases. This is due to the intermolecular structure of the composite. The force between the matrix phase and secondary becomes stronger which allows the hardness of the overall composite to deviate from the theoretical value. Material densification and grain growth are largely affected by the holding time during hot pressing. In the theoretical prediction model, the influence of the grain size is not taken into account. In the experiments, while having different holding times, the composites with same compositions show different grain growth which affects the grain size followed by the hardness of the material. The main function of the theoretical formula for composite materials is to predict the outcome of the multi-phase composite ceramic material. The hardness of the material is little affected by the matrix grain size. The main reason for the change in the hardness of the multi-phase ceramic material is due to the intragranular and intergranuler microstructure.

Chapter # 8: Future Prospects

The theoretical formula has very much eased in predicting the hardness of the multi-phase composite ceramic materials. Although there are still some deviations from the experimental results, but there is also work being done in order to improve the mathematical model so that the theoretical results become more close to the actual experimental results. Composite ceramic materials are now-a-days very important in our daily lives. They are used commonly today in different aspects like cutting, building, coating, etc. If we obtain the desired hardness from the prediction models, it will be easier for the researchers to develop more composite in the future which might enhance our everyday life. The future of composite ceramic materials is very wide and in the near future, we might find everything around us made of composite ceramics due to their excellent physical, thermal, chemical properties.

Chapter # 9: References

[1] V.A. Izhevskiy, L.A. Genova, J.C. Bressiani, F. Aldinger, Progress in SiAlON ceramics, J. Eur. Ceram. Soc. 20 (2000) 2275–2295. https://doi.org/10.1016/S0955-2219(00)00039-X.

[2] J.P. Harkins, National aeronautics and space administration, Environ. Manage. 1 (1977) 9–13. https://doi.org/10.1007/BF01867395.

[3] H. Peng, Spark Plasma Sintering of Si_3N_4 -Based Ceramics Department of Inorganic Chemistry, 2004.

[4] M.H. Bocanegra-Bernal, B. Matovic, Mechanical properties of silicon nitride-based ceramics and its use in structural applications at high temperatures, Mater. Sci. Eng. A. 527 (2010) 1314–1338. https://doi.org/10.1016/j.msea.2009.09.064.

[5] B.A. Ahmed, A.S. Hakeem, T. Laoui, M. Al Malki, M.A. Ehsan, S. Ali, Low-temperature spark plasma sintering of calcium stabilized alpha sialon using nano-size aluminum nitride precursor, Int. J. Refract. Met. Hard Mater. 71 (2018) 301–306. https://doi.org/10.1016/j.ijrmhm.2017.11.009.

[6] C. Santos, C.A. Kelly, S. Ribeiro, K. Strecker, J.V.C. Souza, O.M.M. Silva, α-SiAlON-SiC composites obtained by gas-pressure sintering and hot-pressing, J. Mater. Process. Technol. 189 (2007) 138–142. https://doi.org/10.1016/j.jmatprotec.2007.01.015.

[7] G.Z. Cao, a'-Sialon Ceramics:, (1991) 242–252.

[8] R. Riedel, I.-W. Chen, Ceramics Science and Technology, Volume 1: Structures, Wiley, 2008.

[9] Z.J. Shen, M. Nygren, T. Ekstrom, o.-SIALON GRAINS WITH HIGH ASPECT RATIO-UTOPIA OR REALITY?, (n.d.) 169–178.

[10] D. Salamon, P. Šajgalík, M. Liška, Mechanical Properties and Microstructure of α-SiAlON Based Cutting Tools, Key Eng. Mater. 290 (2005) 250–253. https://doi.org/10.4028/www.scientific.net/kem.290.250.

[11] M.A. Moore, F.S. King, Abrasive wear of brittle solids, Wear 60 (1980) 123–140.

[12] I.M. Hutchings, Wear-resistant materials: into the next century, Mater. Sci. Eng. A

184 (1994) 185–195.

[13] S. Amini, M.H. Fatemi, R. Atefi, High speed turning of Inconel 718 using ceramic and carbide cutting tools, Arab. J. Sci. Eng. 39 (2014) 2323–2330.

[14] J. Deng, T. Cao, L. Liu, Self-lubricating behaviors of Al_2O_3/TiB_2 ceramic tools in dry high-speed machining of hardened steel, J. Eur. Ceram. Soc. 25 (2005) 1073–1079.

[15] R.W. Rice, C.C. Wu, F. Borchelt, Hardness-Grain-Size relations in ceramics, J. Am. Ceram. Soc. 77 (1994) 2539–2553.

[16] C. Pecharromán, F. Esteban-Betegón, J.F. Bartolomé, G. Richter, J.S. Moya, Theoretical model of hardening in Zirconia-Nickel nanoparticle composites, Nano Lett. 4 (2004) 747–751.

[17] M. Kanamaru, T. Tatsuno, T. Kusaka, Hot-Pressed Al_2O_3/SiC whisker/TiC nanocomposites, J. Ceram. Soc. Jpn. 100 (1992) 408–412.

[18] J.P. Singh, Proceedings of the 21st annual conference on composites, advanced ceramics, materials, and structures-A, in: M. Jiang, K.C. Goretta, D. Singh, J.L. Routbort, J.J. Schldies (Eds.), Solid-Particle Erosion of an Al_2O_3-SiC-TiC Composite, John Wiley & Sons, Inc, New Jersey, 1997, pp. 239–246.

[19] G. Zhao, C. Huang, N. He, H. Liu, B. Zou, Microstructure and mechanical properties at room and elevated temperatures of reactively hot pressed TiB2-TiCSiC composite ceramic tool materials, Ceram. Int. 42 (2016) 5353–5361.

[20] J. Song, C. Huang, B. Zou, H. Liu, J. Wang, Microstructure and mechanical properties of TiB2-TiC-WC composite ceramic tool materials, Mater. Des. 36 (2012) 69–74.

[21] J. Watts, G. Hilmas, W.G. Fahrenholtz, Mechanical characterization of ZrB2-SiC composites with varying SiC particle sizes, J. Am. Ceram. Soc. 94 (2011) 4410–4418.

[22] Z. Yin, C. Huang, B. Zou, H. Liu, H. Zhu, J. Wang, Preparation and characterization of Al2O3/TiC micro-nano-composite ceramic tool materials, Ceram. Int. 39 (2013) 4253–4262.

[23] D.J. Scott, P.V. Coveney, J.A. Kilner, J.C.H. Rossiny, N.M.N. Alford, Prediction of the functional properties of ceramic materials from composition using artificial neural networks, J. Eur. Ceram. Soc. 27 (2007) 4425–4435.

[24] R. Stadelmann, M. Lugovy, N. Orlovskaya, P. Mchaffey, M. Radovic, V.M. Sglavo, S. Grasso, M.J. Reece, Mechanical properties and residual stresses in ZrB_2-SiC spark plasma sintered ceramic composites, J. Eur. Ceram. Soc. 36 (2016) 1527–1537.

[25] T. Mori, K. Tanaka, Average stress in matrix and average elastic energy of materials with misfitting inclusions, Acta Metall. 21 (1973) 571–574.

[26] W.H. Bowyer, M.G. Bader, On the re-inforcement of thermoplastics by imperfectly aligned discontinuous fibres, J. Mater. Sci. 7 (1972) 1315–1321.

[27] P. Loginov, L.M. Jr, E. Levashov, M. Petrzhik, Diamond and cBN hybrid and nanomodified cutting tools with enhanced performance: development, testing and modelling, Mater. Des. 88 (2015) 310–319.

[28] Y. Tian, B. Xu, Z. Zhao, Microscopic theory of hardness and design of novel superhard crystals, Int. J. Refract. Met. Hard Mater. 33 (2012) 93–106.

[29] F. Gao, J. He, E. Wu, S. Liu, D. Yu, D. Li, S. Zhang, Y. Tian, Hardness of covalent crystals, Phys. Rev. Lett. 91 (2003) 015502.

[30] A. Simunek, J. Vackar, Hardness of covalent and ionic crystals: first-principle calculations, Phys. Rev. Lett. 96 (2006) 085501.

[31] K. Li, X. Wang, F. Zhang, D. Xue, Electronegativity identification of novel superhard materials, Phys. Rev. Lett. 100 (2008) 235504.

[32] A. Szymański, J.M. Szymański, Hardness Estimation of Minerals, Rocks and Ceramic Materials, Elsevier, Amsterdam, 1989.

[33] S. Dong, D. Jiang, S. Tan, J. Guo, Hot isostatic pressing and post-hot isostatic pressing of SiC-β-sialon composites, Mater. Lett. 29 (1996) 259–263. https://doi.org/10.1016/S0167-577X(96)00155-3.

[34] N.Z. Khalil, S.K. Vajpai, M. Ota, K. Ameyama, Effect of particle size distribution on SiC ceramic sinterability, Funtai Oyobi Fummatsu Yakin/Journal Japan Soc. Powder Powder Metall. 64 (2017) 281–287. https://doi.org/10.2497/jjspm.64.281.

[35] H.W.G. An, Y.C.N.G. He, B.C.M.U. Ddle, L.G. Ao, Microstructure and mechanical properties of nanoscale SiC / Ca -SiAlON composites, 2 (1800) 3263–3269.

[36] J.V.C. Souza, C. Santos, C.A. Kelly, O.M.M. Silva, Development of α-SiAlON-SiC ceramic composites by liquid phase sintering, Int. J. Refract. Met. Hard Mater. 25 (2007) 77–81. https://doi.org/10.1016/j.ijrmhm.2006.01.004.

[37] L. Liu, F. Ye, Z. Zhang, Y. Zhou, Elongation of α-SiC particles in spark plasma sintered α-SiAlON/α-SiC composites, J. Am. Ceram. Soc. 94 (2011) 336–339. https://doi.org/10.1111/j.1551-2916.2010.04296.x.

[38] R.M.A. Khan, B.A. Ahmed, M.M. Al Malki, A.S. Hakeem, T. Laoui, Synthesis of hard and tough calcium stabilized α-sialon/SiC ceramic composites using nano-sized precursors and spark plasma sintering, J. Alloys Compd. 757 (2018) 200–208. https://doi.org/10.1016/j.jallcom.2018.05.062.

[39] S. Li, N. Xu, B. Duan, Y. Li, Effects of added al powder on the properties of sialon-zrn composites fabricated by aluminothermic reduction and nitridation, InterCeram Int. Ceram. Rev. 64 (2015) 119–121. https://doi.org/10.1007/bf03401113.

[40] Z.S. N, A. Maglica, K. Krnel, I. Priboši, T. Kosma, Preparation and properties of β - SiAlON / ZrN nano-composites from, (2007) 49–55.

[41] N.C. Acikbas, S. Tegmen, S. Ozcan, G. Acikbas, Thermal shock behaviour of α:β-SiAlON-TiN composites, Ceram. Int. 40 (2014) 3611–3618. https://doi.org/10.1016/j.ceramint.2013.09.064.

[42] T. Ekström, M. Nygren, SiAION Ceramics, J. Am. Ceram. Soc. 75 (1992) 259–276. https://doi.org/10.1111/j.1151-2916.1992.tb08175.x.

[43] Y. Li, Z. Huang, Y. Xu, M. Fang, Y.G. Liu, J. Yang, X. Hu, Synthesis of ZrN-sialon composites from zircon and alumina by carbothermal reduction-nitridation, Mater. Res. Bull. 47 (2012) 3273–3276. https://doi.org/10.1016/j.materresbull.2012.08.001.

[44] A.R.B. Mei, Lattice dynamics and electron/phonon interactions in epitaxial transition-metal nitrides, 2015. http://hdl.handle.net/2142/87950.

[45] G. Ghosh, S. Vaynman, M.E. Fine, Microstructure of a sialon composite prepared by hot pressing and reactive sintering of β-Si3N4 coated with amorphous Al2O3, Ceram. Int. 25 (1999) 649–659. https://doi.org/10.1016/S0272-8842(98)00079-0.

[46] Z. Shen, Z. Zhao, H. Peng, M. Nygren, Formation of tough interlocking microstuctures in

silicon nitride ceramics by dynamic ripening, Nature. 417 (2002) 266–269. https://doi.org/10.1038/417266a.

[47] L. Yin, M.I. Jones, The formation and properties of Sialon-ZrN composites produced by reaction bonding combined with post gas-pressure sintering, Ceram. Int. 44 (2018) 10753–10761. https://doi.org/10.1016/j.ceramint.2018.03.112.

[48] J.E. Gilbert, A. Mosset, Pergamon PREPARATION OF fK3AION FROM COAL-MINE SCHISTS, Mater. Res. 32 (1997) 1441–1448.

[49] S.K. Andersson, Ö. Staaf, P.O. Olsson, A. Malmport, C.G. Ribbing, Infrared properties of β-sialon as a function of composition, Opt. Mater. (Amst). 10 (1998) 85–93. https://doi.org/10.1016/S0925-3467(97)00146-8.

[50] L. Yin, W. Gao, M.I. Jones, Wear behaviour and electrical conductivity of β-Sialon-ZrN composites fabricated by reaction bonding and gas pressure sintering process, Ceram. Int. 45 (2019) 2266–2274. https://doi.org/10.1016/j.ceramint.2018.10.140.

[51] D. Zheng, X. Li, X. Ai, C. Yang, Y. Li, Bulk WC–Al_2O_3 composites prepared by spark plasma sintering, Int. J. Refract. Metals Hard Mater. 30 (2012) 51–56.

[52] H. Qu, S. Zhu, P. Di, C. Ouyang, Q. Li, Microstructure and mechanical properties of WC–40 vol% Al2O3 composites hot pressed with MgO and CeO_2 additives, Ceram. Int. 39 (2013) 1931–1942.

[53] N. Lin, Y. He, J. Zou, Enhanced mechanical properties and oxidation resistance of tungsten carbide-cobalt cemented carbides with aluminum nitride additions, Ceram. Int. 43 (2017) 6603–6606.

[54] O. Malek, B. Lauwers, Y. Perez, P. De Baets, J. Vleugels, Processing of ultrafine ZrO_2 toughened WC composites, J. Eur. Ceram. Soc. 29 (2009) 3371–3378.

[55] X. Dai-hong, Z. Fu-qin, L. Wei-hong, Fabrication and characterization of ultrafine WC–8Co–xCeB_6 cemented carbides, Ceram. Int. 37 (2011) 2795–2801.

[56] C.B. Wei, X.Y. Song, S.X. Zhao, L. Zhang, W.B. Liu, In-situ synthesis of WC-Co composite powder and densification by sinter-hip, Int. J. Refract. Metals Hard Mater. 28 (2010) 567–571.

[57] H.-C. Kim, I.-J. Shon, J.E. Garey, Z.A. Munir, Consolidation and properties of binderless sub-micron tungsten carbide by field-activated sintering, Int. J. Refract. Metals Hard Mater. 22 (2004) 257–264.

[58] K. Liu, Z. Wang, Z. Yin, L. Cao, J. Yuan, Effect of Co content on microstructure and mechanical properties of ultrafine grained WC-Co cemented carbide sintered by spark plasma sintering, Ceram. Int. 44 (2018) 18711–18718.

[59] H. Saito, A. Iwabuchi, T. Shimizu, Effects of Co content and WC grain size on wear of WC cemented carbide, Wear 261 (2006) 126–132.

[60] W. Su, Y. Sun, J. Liu, J. Feng, J. Ruan, Effects of Ni on the microstructures and properties of WC–6Co cemented carbides fabricated by WC–6(Co, Ni) composite powders, Ceram. Int. 41 (2015) 3169–3177.

[61] S. Sutthiruangwonga, G. Mori, Corrosion properties of Co-based cemented carbides in acidic solutions, Int. J. Refract. Metals Hard Mater. 21 (2003) 135–145.

[62] D. Zheng, X. Lin, Y. Li, S. Qu, C. Yang, Zirconia-toughened WC with/without VC and Cr_3C_2, Ceram. Int. 40 (2014) 2011–2016.

[63] X. Xia, X. Li, J. Li, D. Zheng, Microstructure and characterization of WC-2.8wt% Al_2O_3-6.8 wt% ZrO2 composites produced by spark plasma sintering, Ceram. Int. 42 (2016) 14182–14188.

[64] M. Radajewski, C. Schimpf, L. Krüger, Study of processing routes for WC-MgO composites with varying MgO contents consolidated by FAST/SPS, J. Eur. Ceram. Soc. 37 (2017) 2031–2037.

[65] K. V. Patel, S. R. Shah, T. Özel, Orthogonal cutting of alloy steel 4340 with microgrooved cutting tools, Procedia CIRP. 82 (2019) 178-183.

[66] A. Sert, O. N. Celik, Characterization of the mechanism of cryogenic treatment on the microstructural changes in tungsten carbide cutting tools, Mater. Charact. 150 (2019) 1-7.

[67] V.V. Chayeuski, V.V. Zhylinski, P.V. Rudak, D.P. Rusalsky, N. Višniakov, O. Černašėjus, Characteristics of ZrC/Ni-UDD coatings for a tungsten carbide cutting tool, Appl. Surf. Sci. 446 (2018) 18-26.

[68] J. Heinrichs, M. Olsson, K. Yvell, S. Jacobson, On the deformation mechanisms of cemented carbide in rock drilling – Fundamental studies involving sliding contact against a rock crystal tip, Int. J. Refract. Metal. Hard Mater. 77 (2018) 141-151.

[69] D. Tkalich, V. A. Yastrebov, G. Cailletaud, A. Kane, Multiscale modeling of cemented tungsten carbide in hard rock drilling, Int. J. Solids Struct. 128 (2017) 282-295.

[70] H-C Kim, I-J Shon, J.E. Garey, Z.A. Munir, Consolidation and properties of binderless sub-micron tungsten carbide by field-activated sintering, Int. J. Refract. Metal. Hard. Mater. 22 (2004) 257–264.

[71] S. Sarkar, M. Biswas, R. Halder, S. Bandyopadhyay, Spark plasma sintering processed α-SiAlON bonded tungsten carbide: Densification, microstructure and tribomechanical properties, Mater. Chem. and Phy. 248 (2020) 122955

[72] S. Sarkar, M. Biswas, R. Halder, S. Bandyopadhyay, Densification, microstructure and tribomechanical properties of SPS processed β-SiAlON bonded WC composites, Int. Journal of Refr. Metals and Hard Mater. (2020). https://doi.org/10.1016/j.ijrmhm.2020.105318

[73] M. Biswas, S. Sarkar, R. Halder, S. Bysakh, K. Muraleedharan, S. Bandyopadhyay, Sintering and characterization of a hard-to-hard configured composite: Spark plasma sintered WC reinforced α-SiAlON, Journal of Phy. and Chem. of Solids 145 (2020) 109548

[74] E. Ayas, A. Kara, H. Mandal, S. Turan, F. Kara, Production of α-β SiAlON–TiN/TiCN composites by gas pressure sintering, Silic. Indus. 69 (2004) 287–292.

[75] R.G. Duan, G. Roebben, J. Vleugels, O. Biest, Optimization of microstructure and properties of insitu formed β-O-SiAlON–TiN composite, Mater. Sci. Eng. A 427 (2006) 195–202.

[76] T. Ekström, P.O. Olsson, β-SiAlON ceramics with TiN particle inclusions, J. Eur. Ceram. Soc. 13 (6) (1994) 551–559.

[77] I. Schulz, M. Herrmann, I. Endler, I. Zalite, B. Speisser, J. Kreusser, Nano Si3N4 composites with improved tribological properties, Lub. Sci. 21 (2009) 69–81.

[78] J. Tatami, E. Kodama, H. Watanabe, H. Nakano, T. Wakihara, K. Komeya, T. Megiro, A. Azushima, Fabrication and wear properties of TiN nanoparticle dispersed Si_3N_4 ceramics, J. Ceram. Soc. Jap. 116 (2008) 749–754.

[79] A. Bellosi, A. Fiegna, A. Giachello, Microstructure and Properties of Electrically Conductive Si3N4–TiN Composites, Elsevier Science Publishers B.V., 1991, pp. 225–234.

[80] B. Bitterlich, S. Bitsch, K. Friederich, SiAlON based ceramic cutting tools, J. Eur. Ceram. Soc. 28 (2008) 989–994.

[81] M. Hadad, G. Blugan, J. Kubler, E. Rosset, L. Rohr, J. Michler, Tribological behavior of Si_3N_4 and Si_3N_4–TiN based composites and multi-layer laminates, Wear 260 (2006) 634–664.

[82] Blugan, G., Kubler, J. Critical Flaw Size Reduction in Commercial Si3N4-TiN Composites for Wear Applications, EMPA, Swiss Federal Laboratories for Materials Testing and Research, Laboratory for High Performance Ceramics. http://www.gruppofrattura.it/ocs/index.php/ICF/ICF11/paper/view/9905/9317.

[83] G. Blugan, M. Hadad, T. Graulea, J. Kuebler, Si3N4–TiN–SiC three particle phase composites for wear applications, Ceram. Int. 40 (2014) 1439–1446.

[84] B. Zou, C. Huang, J. Song, H. Liu, Ho, Zhu, Cutting performance and wear mechanism of Si3N4-based nanocomposite ceramic cutting tool in machining of cast iron, Mach. Sci. Technol. 15 (2) (2011) 192–205.

[85] A. Skopp, M. Woydt, K.-H. Habig, Tribological behavior of silicon nitride unlubricated sliding between 22°C materials under and 1000°C, Wear 181–183 (1995) 571–580.

[86] Y. Imada, The tribological reaction accompanying friction and wear of silicon nitride containing titanium nitride, Trans. ASME 114 (1992) 230–235.

[87] N. C. Acikbas, Tribological behavior of α/β-SiAlON-TiN composites, J. of the Euro. Ceramic Soc. 38 (2018) 2279–2288

CERTIFICATE OF COMPLETENESS

It is hereby certified that the dissertation submitted by NS Muhammad Zubair, Reg No. **00000273564**, Titled: ***Theoretical hardness analysis and experimental verification for SiAlON based nano-composites*** has been checked/reviewed and its contents are complete in all respects.

Supervisor's Name: **Dr. Bilal Ahmed Anjum** Signature: _____

Date: _____